


RESEARCH

Open Access



# Electrophysiological characterisation of intranigral-grafted hiPSC-derived dopaminergic neurons in a mouse model of Parkinson's disease

Béregère Ballion<sup>1\*</sup>, Marie-Laure Bonnet<sup>1,2</sup>, Sébastien Brot<sup>1</sup> and Afsaneh Gaillard<sup>1\*</sup> 

## Abstract

**Background** Parkinson's disease (PD) is a complex neurological disorder characterized by the progressive degeneration of midbrain dopaminergic (mDA) neurons in the *substantia nigra* (SN). This degeneration disrupts the basal ganglia loops, leading to both motor and non-motor dysfunctions. Cell therapy for PD aims to replace lost mDA neurons to restore the DA neurotransmission in the denervated forebrain targets. In clinical trials for PD, mDA neurons are implanted into the target area, the striatum, and not in the SN where they are normally located. This ectopic localisation of cells may affect the functionality of transplanted neurons due to the absence of appropriate host afferent regulation. We recently demonstrated that human induced pluripotent stem cells (hiPSCs) derived mDA progenitors grafted into the *substantia nigra pars compacta* (SNpc) in a mouse model of PD, differentiated into mature mDA neurons, restored the degenerated nigrostriatal pathway, and induced motor recovery. The objective of the present study was to evaluate the long-term functionality of these intranigral-grafted mDA neurons by assessing their electrophysiological properties.

**Methods** We performed intranigral transplantation of hiPSC-derived mDA progenitors in a 6-hydroxydopamine RAG2-KO mouse model of PD. We recorded in vivo unit extracellular activity of grafted mDA neurons in anaesthetised mice from 9 to 12 months post-transplantation. Their electrophysiological properties, including firing rates, patterns and spike characteristics, were analysed and compared with those of native nigral dopaminergic neurons from control mice.

**Results** We demonstrated that these grafted mDA neurons exhibited functional characteristics similar to those of native nigral dopaminergic neurons, such as large bi- or triphasic spike waveforms, low firing rates, pacemaker-like properties, and two single-spike firing patterns. Although grafted mDA neurons also displayed low discharge frequencies below 10 Hz, their mean frequency was significantly lower than that of nigral mDA neurons, with a differential pattern distribution.

\*Correspondence:  
Béregère Ballion  
berengere.ballion@univ-poitiers.fr  
Afsaneh Gaillard  
afsaneh.gaillard@univ-poitiers.fr

Full list of author information is available at the end of the article



© The Author(s) 2025. **Open Access** This article is licensed under a Creative Commons Attribution-NonCommercial-NoDerivatives 4.0 International License, which permits any non-commercial use, sharing, distribution and reproduction in any medium or format, as long as you give appropriate credit to the original author(s) and the source, provide a link to the Creative Commons licence, and indicate if you modified the licensed material. You do not have permission under this licence to share adapted material derived from this article or parts of it. The images or other third party material in this article are included in the article's Creative Commons licence, unless indicated otherwise in a credit line to the material. If material is not included in the article's Creative Commons licence and your intended use is not permitted by statutory regulation or exceeds the permitted use, you will need to obtain permission directly from the copyright holder. To view a copy of this licence, visit <http://creativecommons.org/licenses/by-nc-nd/4.0/>.

**Conclusions** Our findings indicate that grafted mDA neurons exhibit dopaminergic-like functional properties, including intrinsic membrane potential oscillations leading to regular firing patterns. Additionally, they demonstrated irregular and burst firing patterns, suggesting they receive modulatory inputs. However, grafted mDA neurons displayed distinct properties, potentially related to their human origin or the incomplete maturation one year after transplantation.

**Keywords** Parkinson's disease, Cell therapy, hiPSC, Intranigral transplantation, Mouse, Electrophysiology, In vivo

## Background

Parkinson's disease (PD) is a complex neurological disorder characterized by the progressive degeneration of mesencephalic dopaminergic (mDA) neurons in the *substantia nigra* (SN) [1, 2], a loss of dopaminergic innervation in the *caudate putamen* [3] and the emergence of Lewy bodies [4, 5].

### Cell therapy for Parkinson's disease

Due to the selective loss of nigral mDA neurons, a therapeutic strategy has emerged over the past 40 years, focusing on the replacement of lost mDA neurons by functional healthy DA neurons. From the late 1970s, experiments conducted in rodent and non-human primate models of PD provided proof-of-principle that fetal ventral mesencephalic dopaminergic (fv-mDA) neurons, grafted into the striatum, can survive [6] and establish synaptic connections with striatal neurons [7, 8]. Further data showed that fv-mDA neurons released dopamine within the *striatum* [6, 9] and partially improved the variable motor deficits induced by nigrostriatal lesions [10, 11].

Advancements in cell derivation and differentiation have positioned pluripotent stem cells (PSCs) as a promising source of cells for transplantation due to their capacity for self-renewal and differentiation. Differentiation protocols have been developed to generate mDA neurons from human embryonic stem cells (hESCs) [12, 13]. Intrastratial or intranigral graft of hESC-derived mDA neurons has been shown to improve dopamine release and variable motor symptoms in rodent PD models [14, 15]. Other sources of stem cells have also been explored, such as induced pluripotent stem cells (iPSCs) obtained from mouse [16] and human somatic cells (hiPSCs) [17, 18]. In animal models of PD, the therapeutic benefits of grafted mDA neurons derived from hiPSCs have been observed in both rodents [19, 20] and non-human primates [21], including dopaminergic reinnervation of the host brain, restoration of dopamine release and improvements in functional motor activity.

### Electrophysiological activity of grafted neurons

The electrophysiological activity of grafted mDA neurons, derived from fetal mesencephalic tissue or pluripotent stem cells, has mostly been studied in experimental models of intrastratial graft in animal models of PD. Most

of these data concerned ex vivo studies performed on brain slice [22–25], as well as in vitro studies using cell culture [19–21, 26] or co-culture (mDA neurospheres into organotypic striatum) [27] prior to transplantation. To our knowledge, few electrophysiological data are available from in vivo recordings in intrastratial graft [28–30] and even fewer from intranigral transplantations [31]. However, these studies confirmed that grafted neurons exhibit well-known and quite distinctive ex vivo [32, 33] and in vivo [34–36] dopaminergic-like electrophysiological features: large bi- or tri-phasic spike waveforms, low discharge frequencies (0–10 Hz), pacemaker-like properties and alternation between single-spike and bursting activities. They also demonstrated that grafted neurons were integrated into the host brain circuitries. However, although these fundamental data provide insights into the mechanisms underlying neuronal electrical activity and networks, *ex vivo* and *in vitro* electrophysiological studies do not overcome specific technical limits with functional consequences. Among the most significant, the data obtained from in vitro cell cultures do not provide an understanding of the mature functional activity of these neurons, nor their modulation by the host structures. In addition, ex vivo brain slices remain vulnerable with a decrease in tissue survival over time. Furthermore, these reduced biological preparations lack a circulatory system, and replicating dynamic environmental variations (pH, temperature, oxygenation and nutrients) is challenging, influencing the electrophysiological activities. Additionally, brain tissue slices do not maintain the complete functional inputs and outputs required for the regulation of neural networks.

### Limitations of intrastratial transplantation

Experiments performed in animal models of PD have provided proof-of-principle that embryonic ventral mesencephalic tissue grafted into the striatum can survive, reinnervate the striatum and improve motor function [37, 38]. Encouraged by these results, clinical trials involving intrastratial transplantation of human fetal VM cells in patients with PD were initiated. The results of clinical trials have shown that DA cell grafts exhibit long-term survival, re-innervate the denervated striatum and, in some patients, induce major long-lasting improvement [39–42]. Despite the beneficial effects observed in many patients, intrastratial transplantation has several

limitations. This ectopic localization of cells may affect the functionality of transplanted neurons due to the lack of appropriate host afferent regulatory inputs from the host [14, 43]. Two concomitant studies published by our group and the Björklund group, showed for the first time that foetal mDA neurons grafted into the SN in animal models of PD can form axonal projections to the striatum, resulting in increased striatal dopamine levels and amelioration of motor deficits [12, 44]. In addition, we demonstrated that only intranigral grafts were capable of both promoting better survival of dopaminergic neurons and inducing recovery of fine motor skills while normalizing cortico-striatal responses [45]. Neuroanatomical and functional restoration of the degenerated nigrostriatal pathway was later confirmed using mDA neurons derived from human pluripotent stem cells grafted into the SN in animal models of PD [46–49]. Overall, these findings demonstrate the ability of intranigral dopaminergic neuron transplants to repair the damaged nigrostriatal pathway in a more physiological way in animal models of PD. This promising approach requires further investigation to improve the efficacy of transplantation for a future clinical applications in patients [14, 43].

#### Long-term evaluation of grafted mDA cells

A fundamental consideration was the long-term therapeutic potential of human pluripotent stem cell-derived mDA neurons in animal models of PD. To date, most transplantation studies using mDA derived from human pluripotent stem cells have not analyzed graft maturation and functionality beyond 6 months post-transplantation (MPT) [19, 48, 50–53]. Given the extended duration of neuronal development and maturation in human, these grafted mDA neurons do not reach fully maturity immediately after transplantation. Indeed, their integration into neural networks requires the establishment of functional interactions with the host's brain structures. This is crucial to ensure and assess (1) the effectiveness of the therapy (2), the stability and persistence of the graft (3), the absence of long-term adverse effects (tumor formation or immune responses), and also (4) the regeneration of functional neural connections, particularly in the nigrostriatal pathway.

In light of these considerations, we performed *in vivo* electrophysiological recordings of mDA neurons derived from hiPSCs transplanted into the SNpc in an immunodeficient mouse model of PD. The grafted mDA neurons used in this study were generated in our laboratory and have been extensively characterized *in vitro* and *in vivo* following transplantation [46].

## Methods

### In vitro generation of mDA precursors

The reprogramming of human fibroblasts into hiPSCs and their subsequent differentiation into mDA precursors were fully described in our previous publication [46]. Briefly, the fibroblasts were obtained from dermis biopsy (Fig. 1A) and reprogrammed into hiPSCs using the StemMACS iPSC mRNA Reprogramming kit over a period of 14 consecutive days (Fig. 1B). The genetic stability of hiPSCs was assessed by the Stemgenomics (iCS-digital PSC 24-probes kit, Montpellier, France). Subsequently, the differentiation of hiPSCs into mDA progenitors was carried out over 26 consecutive days (Fig. 1C) using the PSC Dopaminergic Neuron Differentiation Kit (A3147701, Thermo Fisher Scientific, Waltham, MA, USA). The hiPSCs were initially incubated in floor plate (FP) specification medium for 10 days, yielding predominantly multipotent FP neural stem cell progenitors. Following an 11-day expansion phase, the FP progenitor cells were seeded into complete maturation medium for 5 additional days, reaching the D26 differentiation stage, developmental stage used for transplantation.

### Animals and exclusion/inclusion criteria

This study was conducted in accordance with the ARRIVE 2.0 guidelines. Animal experimental procedures and housing were conducted in compliance with the European Communities Council Directive (2010/63/EU). Every effort was made to reduce the number of animals used and to minimize animal suffering. To ensure their well-being, the mice were monitored daily throughout the procedure for any signs of distress or abnormal behavior. The following signs of pain or discomfort were carefully observed: isolation, reduced activity, altered gait, impaired mobility and hunched posture. If any of these signs appeared, the animal was closely monitored, and a subcutaneous injection of analgesic (ketoprofen, 5 mg/kg) was administered. This injection was repeated twice at 24-hour intervals if necessary. If the animal's condition did not return to normal within 72 h (end-point), euthanasia was performed. In this study, no animals were euthanized under the endpoints established in our research protocol, which was approved by the ethics committee (see 'Declarations' section).

During all surgeries, analgesia was administered, and postoperative analgesic treatment was provided for 48 h.

All tag-identified mice were housed 5 per cage under an inverse 12-hour light/dark cycle in a temperature- and humidity-controlled environment. Housing and husbandry conditions were optimized environmental enrichment such as nesting materials and tunnels. Animals had *ad libitum* access to food and water. In this study, we used 57 (29 males / 28 females) RAG2 KO mice (B6.Cg-Rag2tm1.1Cgn/J; Stock #008449, Jackson Laboratory, Bar

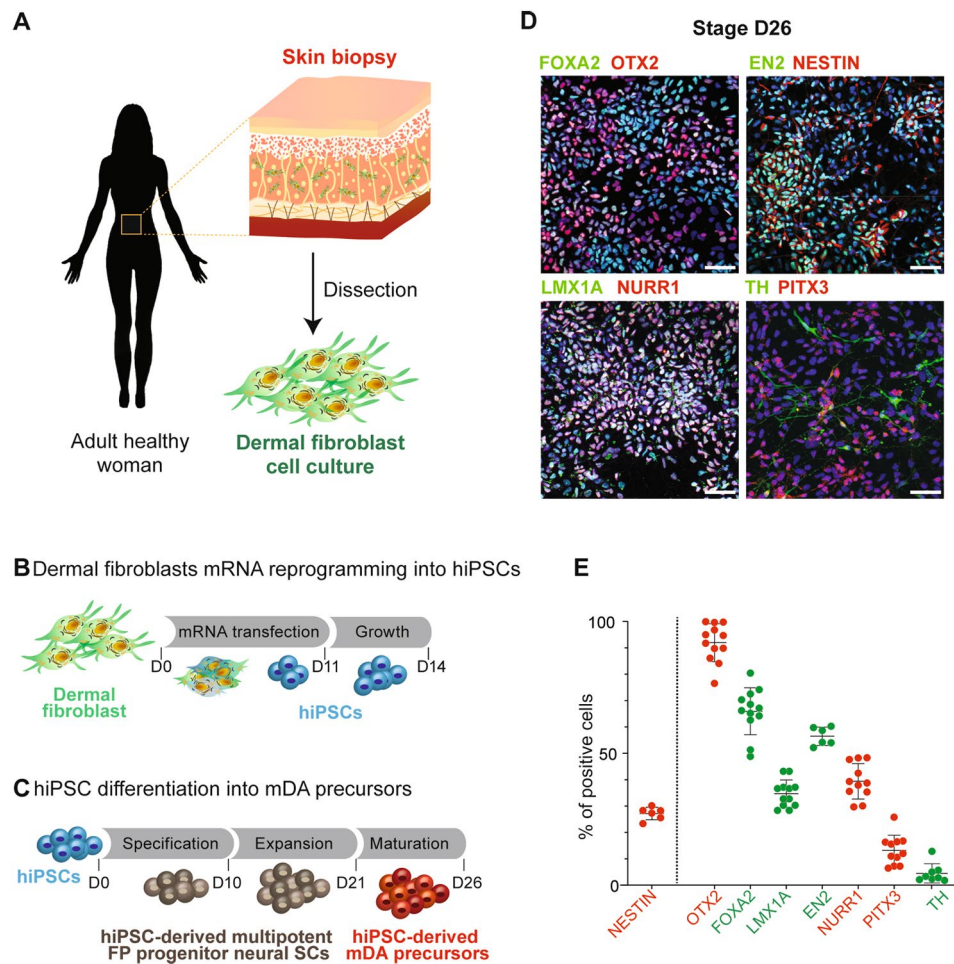


**Fig. 1** In vitro generation of hiPSC-derived mDA precursors. **(A)** Human fibroblasts were obtained from a skin biopsy following an abdominoplasty performed on a healthy 28-year-old woman. **(B)** Dermal fibroblasts were reprogrammed into hiPSCs using mRNA transfection factors. **(C)** Schematic representation of the different stages (specification, expansion, and neuronal maturation) involved in the differentiation of hiPSCs into mesencephalic dopaminergic precursors. At the end of the differentiation stage on day 26 (D26), generated mDA precursors were generated and used for transplantation. **(D)** Representative images of immunolabeling on day 26, showing the expression of floor plate specification markers (OTX2, FOXA2, LMX1A), as well as DA precursor markers (EN2, NURR1 and PITX3), DA neuronal marker (TH) and the neural progenitor identity marker (NESTIN). Cell nuclei were counterstained with DAPI (blue). Scale bars: 50  $\mu$ m. **(E)** Quantitative analysis of different markers expressed by DA precursors at day 26. Data are presented as mean  $\pm$  SD ( $n = 3$  independent experiments, with  $\geq 8000$  cells analyzed per experiment)

Harbor (ME) USA), which exhibit an immune-deficient phenotype (lacking mature T and B cells) [54]. The animals originated from multiple litters with different parents. To eliminate any potential ‘sex effect,’ we ensured that nearly equal numbers of males and females were included in each of the 2 experimental groups. Allocation of animals to each group was not performed using a mathematical randomisation technique but rather by cage, grouping animals of the same sex but from different litters.

Our study design aimed to compare the in vivo electrophysiological spontaneous activity of nigral dopaminergic neurons in control mice (control group:  $n = 16$ ; 8 males / 8 females) with that of hiPSC-derived dopaminergic neurons transplanted into the SNpc of an immunodeficient mouse model of PD (grafted group:  $n = 41$ ; 23

males / 18 females). The control group was independent of the grafted group, and each group represented a distinct experimental condition. Each animal was treated as an experimental unit. For each experimental unit, an inclusion criterion was defined based on a minimum number of neurons recorded per animal (i.e. at least three stable neurons) to ensure the quality of the spontaneous activity recordings, particularly by verifying the absence of artefacts. The recorded spontaneous activities were initially analyzed in real-time during electrophysiological experiments by assessing the stability of neuronal activity (discharge frequency) and spike parameters to confirm the reliability of the recordings. For this reason, 17 mice were excluded: 3 in the control group (1 showing no electrophysiological spontaneous activity and 2 with unstable spontaneous activity), and 14 in the grafted



group (10 showing no electrophysiological spontaneous activity and 4 with single unstable spontaneous activity). Post-mortem immunohistochemical analysis revealed that the excluded grafted animals had either a small or a misplaced transplant.

Finally, the last exclusion criterion involved the phenotype identification of the recorded neurons, using intracellular neurobiotin injection following the electrophysiological recordings to ensure that the neurobiotin-filled neuron was a dopaminergic neuron. This procedure was a delicate and limiting step, considering that 26% and 48% of injected neurons did not survive to the injection procedure in the control and grafted groups, respectively. As a result, the restrictive immunohistochemical identification of putative dopaminergic neurons led to a retrospective electrophysiological data analysis from only 25 mice (11 control: 6 males and 5 females / 14 grafted: 7 males and 7 females). Thus, we analysed 20 neurons in the control group and 18 neurons in the grafted group.

Electrophysiological recordings were conducted in 3- to 7-month-old control mice and from the 9th to the 12th MPT in grafted group.

#### 6-OHDA lesion and transplantation procedures

The experimental procedures were performed over a 3-week period (Fig. 2).

Adult mice (weight: 20 to 29 g, 4–6 months old,  $n=41$ ; 23 males, 18 females) were anesthetized and fixed on a stereotaxic frame and unilaterally lesioned by 6-hydroxydopamine (6-OHDA) injection into the SNpc (Fig. 2A), as previously described [12]. 6-OHDA (8  $\mu\text{g}/\mu\text{l}$ , Sigma-Aldrich, H116) was dissolved in 0.9% saline solution containing 0.1% ascorbic acid (Sigma-Aldrich, A5960), and 1  $\mu\text{l}$  was injected slowly with a 5  $\mu\text{l}$  Hamilton syringe into the left SNpc at the following stereotaxic coordinates relative to bregma according to the Mouse Brain Atlas [55]: Antero-posterior (AP) = -3.2 mm, Medio-lateral (ML) = 1.4 mm, Dorso-ventral (DV) = -3.8 mm. Three weeks post-6-OHDA injection, 1  $\mu\text{l}$  of hiPSC-derived mDA progenitor suspension (100,000 cells/ $\mu\text{l}$ ) was injected into the SNpc at the same coordinates used for 6-OHDA injection (Fig. 2B). Both the 6-OHDA injection and the hiPSC-derived mDA progenitor transplantation were performed under intraperitoneal (I.P.) anesthesia using ketamine hydrochloride (100 mg/kg) and xylazine hydrochloride (10 mg/kg). In vivo electrophysiological recordings were performed in the grafted mice between the 9th and 12th MPT.

#### In vivo single-unit extracellular recordings

All mice included in this study ( $n=57$ ) were anaesthetized with 5% isoflurane (Iso-Vet, Piramal) and fixed on a stereotaxic frame. Corneal dehydration was prevented by the application of ophthalmic lubrication gel

(Ocrigel™, TVM Lab). Since temperature is an influential variable affecting dopaminergic neuron homeostasis and membrane excitability [56], body temperature was maintained at  $37.5 \pm 0.5$  °C using a homeothermic heating pad. Local anaesthetic lidocaine (Lidor® 20 mg/ml, Richter pharma) was infiltrated subcutaneously before making a sagittal incision to expose the cranial bone. According to the stereotaxic coordinates [55], a drill hole was made in the skull just above the SNpc to pass-through extracellular recording electrode. Extracellular recording electrodes were prepared using glass micropipettes (13–26 M $\Omega$  impedance; 1.4  $\mu\text{m}$  tip external diameter) pulled from capillaries (GC150F, Harvard Apparatus) and filled with 0.4 M NaCl containing 2% neurobiotin (Vector Laboratories). To cover a wide spatial field of interest (SNpc or transplant), recording electrodes were lowered under stereotaxic guidance in multiple tracks separated by 0.1 mm-step from initial coordinates (-3.16 mm posterior to bregma, 1.3 mm from the midline). In control mice, electrodes were lowered in 12 tracks through the SNpc (Fig. 3A) from -3.9 mm to -4.4 mm below the brain surface (Fig. 3B). In grafted mice, the transplant covered a wider brain area than the SNpc, so the recording area was more extensive and spanned 18 tracks (Fig. 3C) between -3.6 mm to -4.6 mm ventral to the brain surface (Fig. 3D). The single-unit electrical activity recorded was initially amplified 10 times and bandpass-filtered (low pass 30–300 Hz; high pass 16 kHz). Before being digitized at 16 kHz (CED 1401, Cambridge Electronics Design), the signal was further amplified 50 times (Multiclamp 700b, Axon Instruments), free from electrical interferences and 50 Hz noise (HumBug, Quest Scientific), and finally displayed on Spike 2 7.0 software (Cambridge Electronics Design). Spontaneous unit activity was recorded for a 300-second period, and an initial putative dopaminergic neuron identification was performed based on well-established parameters [57, 58] (Fig. 4AC): wide bi- or tri-phasic action potential (duration > 2 ms), a notch or inflection with varying amplitude in rising positive phase, and a prominent negative phase. A supplementary conservative time duration was analysed between spike initiation and its maximal negative phase. For dopaminergic neurons, this latter criterion was described as being over 1.1 ms [59–61]. Additionally, dopaminergic neurons were assumed to display a slow firing rate (up to 10 Hz) and high-frequency burst firing (2 to 10 spikes with decreasing amplitude and increasing consecutive interspike intervals) [57, 58]. After recording session, neurobiotin was juxtacellularly injected to confirm *a posteriori* the electrophysiological dopaminergic identification [62–64]. Briefly, the glass micropipette was advanced very close to the cell, and increasing iontophoretic positive currents were applied (1–10 nA, 250

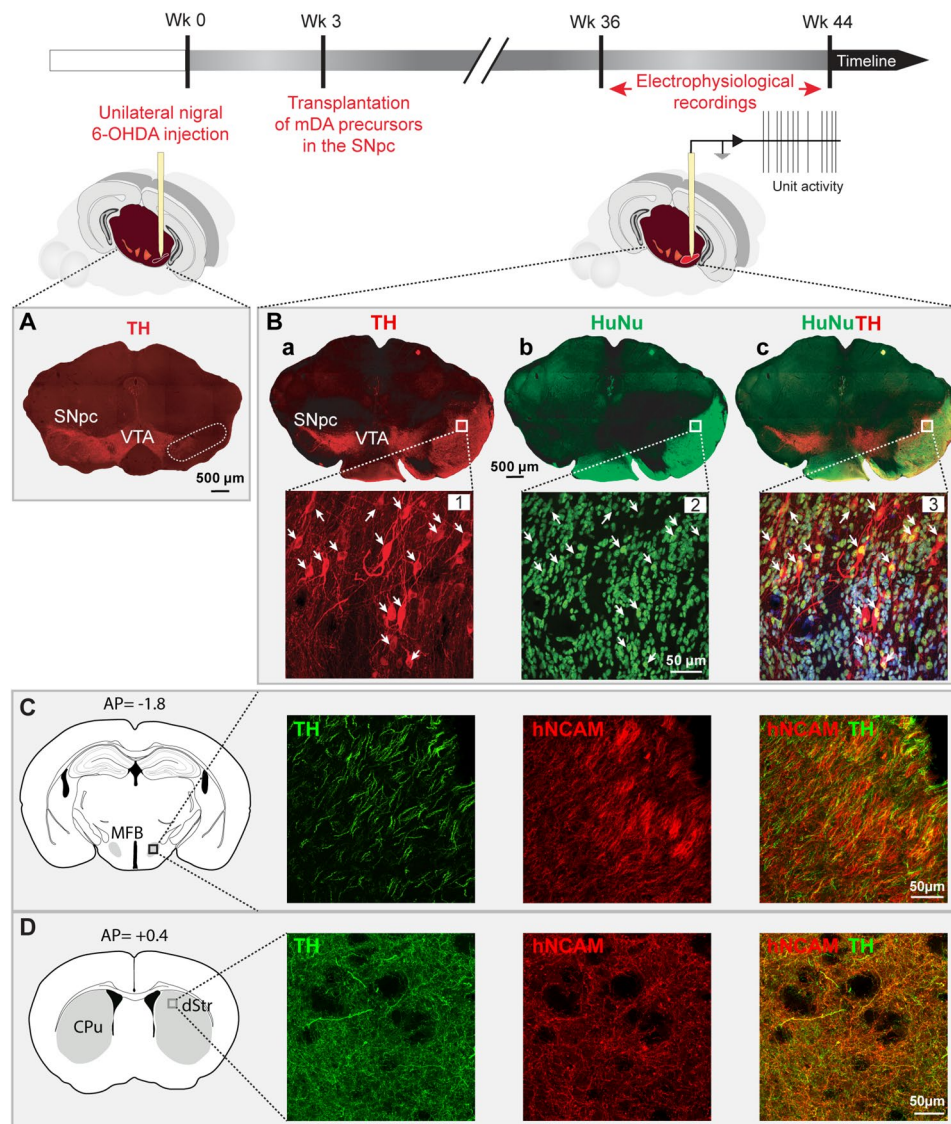


**Fig. 2** Illustrations of experimental timeline and visualisation of grafted mDA neurons in the host brain. 6-hydroxydopamine (6-OHDA) was injected unilaterally into the left SNpc at week 0 (Wk 0). Three weeks later (Wk 3), dopaminergic precursors derived from hiPSCs were transplanted into the same area. In vivo extracellular electrophysiological recordings were performed between 9 months (Wk 36) and 12 months (Wk 44) post-transplantation. **(A)** Coronal brain section showing dopamine cell loss induced by the 6-OHDA injection into the left SNpc. **(B)** Representative images of TH<sup>+</sup> and HuNu<sup>+</sup> neurons within the graft, 9 months after transplantation. The labelling shows the localisation of TH<sup>+</sup> neurons (in red, **a**), the transplant identified by HuNu nuclear labelling (in green, **b**), and the merged image of the TH<sup>+</sup>/HuNu<sup>+</sup> (**c**). High-magnification images within the white frame highlight TH<sup>+</sup> neurons [1], HuNu<sup>+</sup> cells [2], and TH<sup>+</sup> neurons derived from hiPSCs (indicated by white arrows) in [3]. **(C, D)** Representative images of double immunostainings for TH (green) and hNCAM (red) along the nigrostriatal pathway through the medial forebrain bundle (MFB) (**C**; AP: -1.8 from bregma) and in the dorsal striatum (dStr) (**D**; AP: +0.4 from bregma) at 12 months after transplantation. Double-labeled TH<sup>+</sup>/hNCAM<sup>+</sup> fibers indicate axonal projections originating from human grafted mDA-neurons. The schematic drawings were adapted from *The Paxinos and Franklin's mouse brain atlas* [55]. Abbreviations: SNpc, substantia nigra pars compacta; VTA, ventral tegmental area; AP, antero-posterior; CPu, caudate putamen; MFB, medial forebrain bundle; dStr, dorsal striatum

ms, 50% firing rate) until they robustly drove the firing activity for 2 to 5 min to achieve diffused labelling.

The surgical procedures and electrophysiological recording sessions were performed under isoflurane maintenance of 2.5% and 1.5 to 2%, respectively.

#### Measures of electrophysiological data

Electrophysiological parameters were obtained from 150 to 180 consecutive seconds of recordings exhibiting stable spontaneous firing activity. Recordings of dopaminergic-identified neurons were analysed off-line using Spike 2 software. Spike duration was calculated from the average waveform of 20 successive discriminated spikes, and three duration parameters were investigated (Fig. 4B in

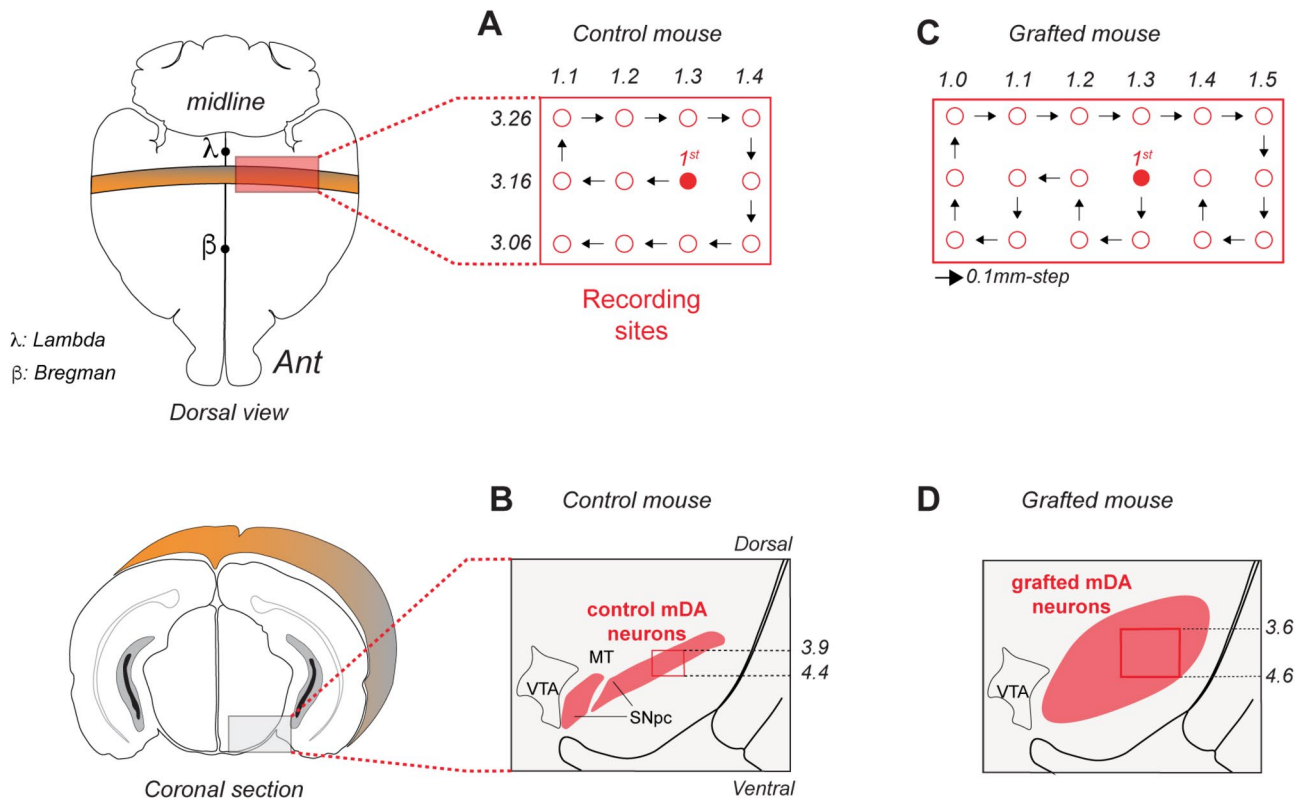


**Fig. 3** Localisation of in vivo extracellular recordings in mouse brain (**A, B**) In control mice, 12 electrode tracks were performed every 0.1 mm-step starting from the initiate coordinates (red point in **A**) and lowered through the *substantia nigra pars compacta* (SNpc) from  $-3.9$  mm to  $-4.4$  mm below the brain surface (**B**). (**C, D**) In grafted mice, the transplant occupied a larger volume than the SNpc. Consequently, 18 electrode tracks were performed (**C**), and lowered across a wider range, from  $-3.6$  to  $-4.6$  mm below the brain surface (**D**). Abbreviations:  $\lambda$ , lambda;  $\beta$ , bregma; Ant, anterior; SNpc, *substantia nigra pars compacta*; VTA, ventral tegmental area; MT, medial terminal nucleus

frame): the total spike duration from the first to the last deviation from baseline (TS), the duration from spike initiation to the maximal negative phase (IS), and finally the half-maximal spike duration (HS), measured between the points at which the spike reached half of its maximum amplitude during both the positive and negative phases. The latter duration is commonly used for human neurons in clinical analysis [65, 66]. The firing rate (Hz) was then averaged from spontaneous discharge activity over at least 150 consecutive seconds.

#### Identification of discharge patterns

Dopaminergic neurons exhibited spontaneous firing patterns that were categorized as either regular or irregular single-spiking firing, or in bursty mode (intermittent high-frequency episodes within single-spiking firings). Pattern identification was assessed using both the specific distribution of interspike intervals (ISI) and the autocorrelogram (AutoC). ISI histograms (ISIH) were used to assess the ISI distribution, with the coefficient of variation (CV) calculated as the ratio between the ISI standard deviation (SD) and the ISI mean. The discharge pattern was classified as regular when the CV was below 0.5 and

irregular when it was above 0.5 [67]. Neurons exhibiting bursty episodes typically displayed CVs close to or above 1. AutoC was used to evaluate the rhythmic properties of regular discharges. Both ISIH and AutoC were traditionally constructed with a 10 ms bin width over a 1-second time interval. However, if mDA or grafted mDA neurons showed a very slow discharge rate, the ISIH and AutoC were extended to 2-second intervals.

#### Identification of burst activity

Bursty episodes have been previously described as a train of 2 or more spikes with a short ISI, followed by a period of inactivity [68]. In this study, we applied this burst identification method since the discharge firing of recorded neurons remained steady overtime (low coefficient of variation) and relatively low, regardless of the single-spike discharge pattern (irregular or regular). These criteria were defined as at least 2 consecutive spikes with an 80 ms maximum ISI to onset the burst and more than 160 ms ISI to end the burst. The bursting potential was evaluated using the percentage of spikes in burst (SIB), referring to the ratio between the number of spikes in bursts and the total number of spikes recorded



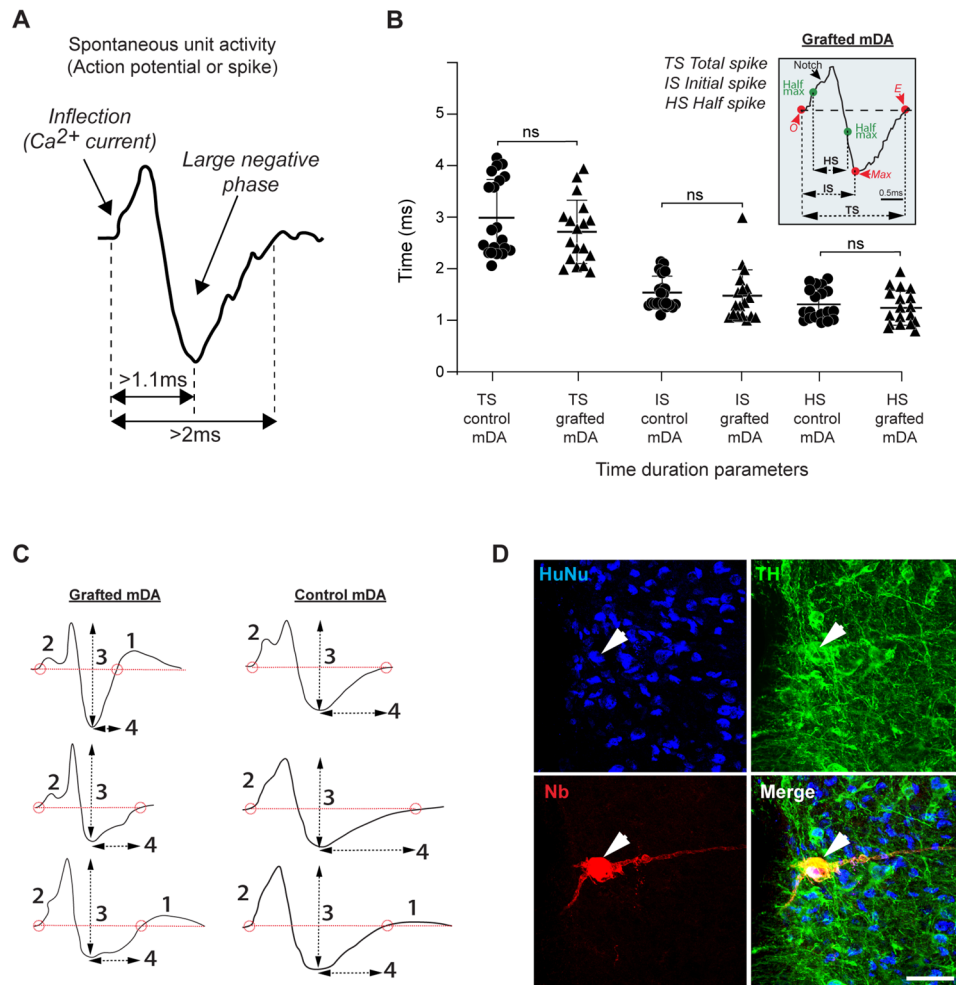


**Fig. 4** Electrophysiological and immunohistochemical identification of dopaminergic neurons. **(A)** Representation of in vivo single action potential (average of 20 successive spike traces) from nigral mDA neuron in control mice. The spike was identified as originating from a dopaminergic neuron based on specific properties, including its large biphasic shape, an inflection on the positive phase driven by a  $\text{Ca}^{2+}$  conductance, and a prominent negative phase. Moreover, the spike time duration exceeded 2 ms, and its initial phase (from the start to the end of hyperpolarisation) had values greater than 1.1 ms. **(B)** Scatterplot representing the distribution of total spike (TS), initial spike (IS), and half spike (HS) durations for 20 control mDA neurons (black dots) and 18 grafted mDA neurons (black triangles), along with their respective mean and SD values. Each plot represents the average of 20 successive spike traces. An unpaired t-test with Welch's correction showed no statistical differences between control mDA and grafted mDA neurons in TS ((t, df) = 1.233, 35.79;  $p = 0.2257$ ), IS ((t, df) = 0.444, 28.11;  $p = 0.6605$ ), and HS ((t, df) = 0.5710, 34.07;  $p = 0.5717$ ). The inset shows an example of the spike waveform recorded from a grafted mDA neuron with the different spike durations (TS, IS, HS). The raw trace represents the average of 20 successive spikes in the recording sequence. **(C)** Spike shape variability in grafted mDA and control mDA neurons. For each experimental condition, three examples of recorded spike shapes are shown. Different representative variant points are annotated: 1 (post-hyperpolarisation rebound), 2 (notch prominence), 3 (amplitude between depolarisation and hyperpolarisation maxima), and 4 (post-hyperpolarisation duration). **(D)** Immunolabelling identification of recorded grafted mDA neurons. The image shows the merging of neurobiotin (Nb)-filled recorded grafted mDA neuron (in red), co-expressing HuNu (in blue) and TH (in green). Scale bar: 50  $\mu\text{m}$

during spontaneous activity. When dopaminergic neurons exhibited bursts, bursting firing analysis was performed to calculate the mean spike number per burst, the mean  $\text{ISI}_1$  to onset a burst, the mean consecutive ISI between spikes within a burst, and the mean intraburst frequency.

#### Tissue processing

After electrophysiological recordings, mice were injected with lethal dose of pentobarbital (60 mg / kg I.P.,

Euthasol®, Virbac, 51311-050-01) and perfused intracardially with 0.9% NaCl solution (100 ml / 37 °C), followed by 4% paraformaldehyde (PFA) (200 ml at 4 °C, Thermo Scientific, A11313-0 C). Brains were removed and kept overnight in 4% PFA at 4 °C before being cryoprotected in 30% sucrose solution for at least 2 days. Brains were then sectioned into 40  $\mu\text{m}$  thick coronal slices and stored in antifreeze solution (20% glucose, 40% ethylene glycol, 0.025% sodium azide, 0.05 M phosphate buffer solution



-PBS-, pH 7.4) at  $-30^{\circ}\text{C}$  before immunohistochemical processing.

### Immunocytochemistry

The list of suppliers and dilutions of antibodies and fluorescent probes was detailed in Additional file 1.

### Immunostaining on hiPSC

The dopaminergic precursor phenotype of the hiPSC culture was validated at the D26 differentiation stage prior to transplantation. Immunostaining was performed to evaluate the expression of transcription factors involved in FP specification (OTX2, FOXA2, and LMX1A), the dopaminergic differentiation pathway (EN2, NURR1 and PITX3), dopamine synthesis regulation (TH) in dopaminergic neurons, and the neural progenitor identity through the expression of NESTIN. Cells grown on coverslips were fixed with 4% EM grade PFA (Electron Microscopy Sciences, Hatfield, PA, USA; RT-15710) for 15 min at room temperature (RT). After 3 washes with 0.1 M PBS (pH 7.4), the cells were first permeabilized and blocked with blocking solution containing 0.1 M PBS, 3% bovine serum, 0.3% Triton X-100 (pH 7.4) for 60 min at RT, and then incubated with appropriate primary antibodies diluted in blocking solution overnight at  $4^{\circ}\text{C}$ . After 3 washes with 0.1 M PBS, the cells were incubated with secondary antibodies in blocking solution for 60 min at RT. Finally, the cells were mounted on microscope slides using 15  $\mu\text{l}$  of Vectashield Vibrance with DAPI (Vector Laboratories, Burlingame, CA, USA; H-1800-10) for fluorescence microscopy observation.

### Immunostaining on brain sections

The dopaminergic identity of *in vivo* recorded neurons was retrospectively confirmed by co-labelling with TH and fluorochrome-conjugated streptavidin to detect neurobiotin injected into neurons after electrophysiological recordings. In transplanted mice, the human origin of the putative recorded grafted mDA neurons was verified by labelling with a human nuclear marker (HuNu). The hNCAM antibody was used to trace the axonal projections of grafted mDA neurons extending fibers through MFB to their primary target structure, the caudate putamen (CPu). In some transplanted mice, the presence of GABAergic neurons was assessed using an antibody against Glutamate decarboxylase 67 (GAD67). Free-floating sections were pre-treated in blocking solution for 90 min at RT before incubation with the primary antibodies of interest, diluted in blocking solution. After overnight incubation at  $4^{\circ}\text{C}$  with agitation and  $3 \times 10$ -minute rinses in 0.1 M PBS, sections were incubated with appropriate secondary antibodies for 90 min at RT. Following 3 10-minute rinses in 0.1 M PBS, sections were incubated for 90 min at RT with appropriate

Alexa Fluor™-conjugated streptavidin in blocking solution to detect neurobiotin. Finally, sections were rinsed three times for 10 min in 0.1 M PBS before being labelled with DAPI solution (1:10,000, Sigma-Aldrich, D9542) for 10 min, rinsed 3 times with 0.1 M PBS, mounted on slides, and coverslipped with DPX Mountant (Sigma-Aldrich, 06522).

### Imaging acquisition and outcome measures

Images were acquired with a Zeiss Axio Imager M2 microscope equipped with an Apotome module (Carl Zeiss Microscopy) using 10x or 20x objectives. Areas of interest were further analyzed with a confocal laser-scanning microscope FV3000 (Olympus). For cell culture analysis, 6 to 8 images per immunostaining and per experiment were captured and quantified. For the localisation of hiPSC-GAD 67<sup>+</sup> and hiPSC-TH<sup>+</sup> neurons within the graft, counting was performed across the entire graft area in 3 to 4 coronal brain sections per mouse. Quantification of nuclear staining was conducted automatically using ImageJ software (Version 1.53c; NIH), while non-nuclear staining was manually quantified using ZEN Blue edition software (V 3.2; Carl Zeiss Microscopy).

### Statistical analyses

Data were expressed as mean  $\pm$  standard deviation (SD). Comparative analyses were performed using Welch's correction unpaired t-test for two-group comparisons and one-way Welch's ANOVA for comparisons involving three or more groups. Welch's correction was applied to analyze the variability between groups. One-way ANOVA with Greenhouse-Geisser correction was used to compare repeated or consecutive measures of a single neuron and to assess variability between neurons. Ordinary two-way ANOVA was employed to evaluate the effects of multiple factors on variables. Chi-square tests were used to compare distributions between populations. Non-parametric tests (Mann-Whitney test, Wilcoxon matched-pairs signed rank test, paired Friedman test) were applied for small sample sizes or non-normal distributions. Statistical significance was considered when  $P < 0.05$ . (\*),  $p < 0.01$  (\*\*),  $p < 0.001$  (\*\*\*) and  $p < 0.0001$  (\*\*\*\*). Graphs and statistical analyses were conducted using GraphPad Prism v 8.4.3.

### Results

In this study, we compared the *in vivo* spontaneous electrophysiological profiles of nigral mDA neurons in control animals and grafted mDA neurons derived from hiPSCs into an animal model of PD after 9 to 12 MPT.

### Specific dopaminergic markers of neurons prior to transplantation

In our previously study we determined D26 as the optimal differentiation stage of DA neurons for transplantation based on the expression levels of specific dopaminergic precursor markers: OTX2, FOXA2, LMX1A (floor plate specification markers), EN2, NURR1, PITX3 (Dopaminergic precursor differentiation markers), and TH (regulatory enzyme of dopamine synthesis). Here, we first confirmed the expression of these dopaminergic precursor biomarkers (Fig. 1D) and their quantitative analysis (Fig. 1E) prior to transplantation. Floor plate specification markers were highly expressed (OTX2:  $91.98 \pm 7.17\%$   $n=12$ ; FOXA2:  $65.96 \pm 8.89\%$   $n=12$ ; LMX1A:  $34.74 \pm 5.13\%$   $n=12$ ). Early dopaminergic differentiation markers (EN2:  $56.51 \pm 3.46\%$   $n=6$ ; NURR1  $39.41 \pm 6.71\%$   $n=11$ ) and late markers (PITX3  $13.24 \pm 5.72\%$   $n=11$ ) revealed a dynamic differentiation process. A small proportion of hiPSC-derived cells began expressing TH biomarkers ( $3.73 \pm 3.67\%$ ;  $n=8$ ). Additionally, approximately a quarter of the transplanted cells retained a neural progenitor identity, as indicated by NESTIN expression (NESTIN  $27.18 \pm 2.38\%$   $n=6$ ).

### Neuronal populations in the transplant

In accord with our previous published results [46], we observed that DA precursors derived from hiPSCs grafted into the SNpc differentiated into both mDA and

GABAergic neurons (Fig. 2B/Fig. 5A) 12 MPT. Quantification of grafted mDA neurons (TH<sup>+</sup>/HuNu<sup>+</sup>) and grafted GABA (GAD 67<sup>+</sup>/HuNu<sup>+</sup>) neurons within the graft revealed that both neuronal types were present in similar proportions:  $9.75 \pm 2.76\%$  ( $n=6$ ; CV=0.28) and  $8.11 \pm 1.41\%$  ( $n=6$ ; CV=0.17), respectively (Fig. 5B).

Intranigral grafts of hiPSC-derived mDA neurons allowed restoration of degenerated nigrostriatal pathways. Indeed, axons of the grafted mDA neurons developed projections through the medial forebrain bundle (Fig. 2C) to the striatum (Fig. 2D). A large number of hNCAM<sup>+</sup>/TH<sup>+</sup> fibers was observed mainly in the dorsolateral striatum (dStr) (Fig. 2D), which represents the main target of A9 neurons from the SNpc.

### Electrophysiological properties of grafted dopaminergic neurons: Spike hallmarks

We investigated the electrophysiological properties of the mDA grafted neurons between the 9th and 12th MPT. This time frame was selected based on our previous published results [46] showing that between the 9th and 12th MPT, functional maturation of grafted neurons and development of axonal projections to the striatum is optimal.

The well-known spike hallmarks (Fig. 4A) served as the primary criteria for identifying putative dopaminergic neurons in both the SNpc and the transplant. The spike waveform was a key feature for dopaminergic neuron

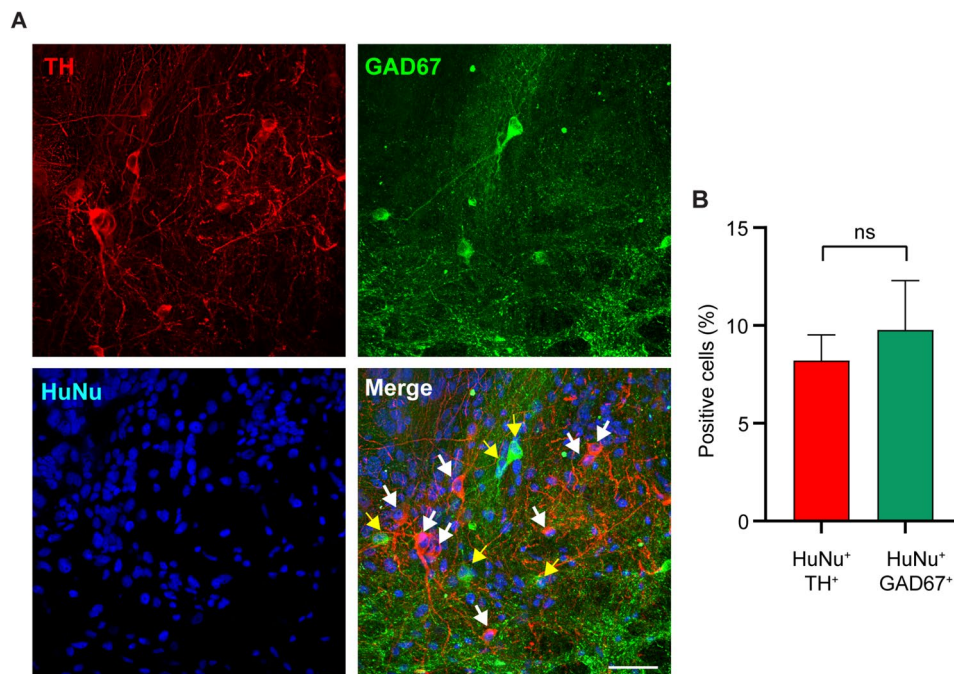


**Fig. 5** Cellular composition of the grafts at 12 MPT. **(A)** Representative immunofluorescence images of TH<sup>+</sup> neurons (in red), GAD67<sup>+</sup> neurons (in green), HuNu<sup>+</sup> neurons (in blue), and merged image illustrating TH<sup>+</sup>/HuNu<sup>+</sup> (indicated by white arrows) and GAD67<sup>+</sup>/HuNu<sup>+</sup> (indicated by yellow arrows) within the graft. Scale bar: 50  $\mu$ m. **(B)** Quantification of cells co-expressing TH<sup>+</sup>/HuNu<sup>+</sup> and GAD67<sup>+</sup>/HuNu<sup>+</sup> neurons within the graft. Data are expressed as mean  $\pm$  SD ( $n=7$  independent experiments with  $\geq 10\,000$  HuNu<sup>+</sup> cells per experiment). Unpaired T-test:  $t=1.301$ ,  $df=10$ ;  $p=0.222$

discrimination with a prominent notch during the depolarisation phase, a pronounced negative phase, and two specific phase durations (Fig. 4B: total spike (TS) and initial spike (IS)). We demonstrated that the total spike duration (TS) was comparable and consistently exceeded 2 ms in both grafted mDA neurons ( $2.72 \pm 0.62$  ms,  $n = 18$  neurons,  $CV = 0.23$ ) and mDA neurons from the control group ( $2.99 \pm 0.74$  ms,  $n = 20$  neurons,  $CV = 0.24$ ). Similarly, the initial spike duration (IS) showed no significant difference between the two populations (mDA neurons  $IS = 1.54 \pm 0.32$  ms,  $n = 20$  neurons,  $CV = 0.20$ ; grafted mDA neurons  $IS = 1.48 \pm 0.50$  ms,  $n = 18$  neurons,  $CV = 0.34$ ).

We also evaluated a third temporal parameter, the spike half-maximal duration (HS in Fig. 4B), a feature of interest in several clinical studies on human dopaminergic neurons. The HS duration was found to be comparable between mDA neurons ( $1.26 \pm 0.30$  ms,  $n = 20$  neurons,  $CV = 0.23$ ) and grafted mDA neurons ( $1.20 \pm 0.34$  ms,  $n = 18$  neurons,  $CV = 0.28$ ).

While the overall spike waveform shape remained consistent across dopaminergic populations, slight variations were observed (Fig. 4C). These differences were independent of the low-pass filter applied during the electrophysiological acquisition process (30 to 300 Hz). Specifically, the spike waveforms could alternate between a biphasic or tri-phasic profile, often characterized by a post-hyperpolarisation rebound (1). During the initial depolarisation segment, the degree of notch prominence varied (2), as did the amplitude ratio between depolarisation and hyperpolarisation phases (3), and the post-hyperpolarisation duration (4).

At the end of the electrophysiological recordings, the identification of the recorded neurons was retrospectively confirmed through immunohistochemical staining of labeled-neurobiotin(Nb)-injected neurons, coexpressing TH in control mDA neurons, and both TH and HuNu in grafted mDA neurons (Fig. 4D).

#### **Electrophysiological properties of dopaminergic grafted neurons: firing patterns**

We found that grafted mDA neurons displayed similar spontaneous activity properties to control mDA neurons (Fig. 6). They could fire in two single-spike patterned discharges (Fig. 6A), either irregular (Fig. 6a) or regular (Fig. 6b), and could intermittently switch into high-frequency burst episodes (Fig. 6c). These data were consistent with those from nigral mDA neurons of control mice (Fig. 6B: irregular in j, regular in k and bursty in l). Discharge patterns were distinguished by the ISI distribution (ISIH), its coefficient of variation (CV), and the spike autocorrelation (AutoC). When irregular (Fig. 6a and j), ISIs were distributed in the 1-second range ( $CV > 0.5$ ) with a peak in the first 250 ms. Simultaneously, AutoC

showed no rhythmicity in discharge activity. Regular (pacemaker-like) patterns (Fig. 6b and k) were identified by an ISI distribution in 100–250 ms time interval ( $CV < 0.5$ ) and two or more peaks at regular intervals in the AutoC, signalling the rhythmic component. During spontaneous activity, some neurons switched to transient bursting episodes (Fig. 6c and l) with a bimodal ISI distribution, including an early peak (below 200 ms) reflecting ISIs within bursts and a later distribution corresponding to intervals between bursts or non-burst-related spikes. Most bursty neurons showed a CV close to or above 1, and no rhythmic activity was detected even if the considered neuron displayed regular discharge activity before evoking bursting events. Note that autocorrelograms could exhibit a variable distribution related to underlying irregular or regular patterned discharge and its level of firing rate. These results indicated that grafted mDA neurons exhibited a firing pattern spectrum similar to that described in control mDA neurons.

Even though the population of grafted mDA neurons tended to exhibit a more tightly clustered frequency range (0.19–5.41 Hz,  $CV = 0.42$ ) compared to mDA neurons (0.47–8.99 Hz,  $CV = 0.64$ ) neurons, the mean discharge frequency was significantly lower ( $p < 0.0001$ ) in grafted mDA neurons ( $2.32 \pm 1.48$  Hz,  $n = 18$ ) than in mDA neurons ( $5.17 \pm 2.17$  Hz,  $n = 20$ ) (Fig. 7A). Since grafted mDA neurons exhibited a reduced discharge rate, we examined whether the discharge frequency was related to the firing pattern (Fig. 7B). Overall, ANOVA comparison revealed that both the firing patterns (regular vs. irregular) and the experimental conditions (control mDA vs. grafted mDA) strongly affected the firing rate ( $p = 0.0029$  \*\*). More precisely, nigral mDA neurons displayed similar mean discharge rates and value distributions regardless of the discharge pattern considered (irregular  $4.94 \pm 2.17$  Hz,  $n = 12$ ,  $CV = 0.44$  vs. regular  $5.26 \pm 2.31$  Hz,  $n = 8$ ,  $CV = 0.44$ ;  $p = 0.76$ ). In contrast, irregular grafted mDA neurons exhibited a lower mean firing rate compared to regular grafted mDA neurons (irregular  $1.88 \pm 1.60$  Hz,  $n = 12$ ,  $CV = 0.85$  vs. regular  $3.19 \pm 0.69$  Hz,  $n = 6$ ,  $CV = 0.2$ ;  $p = 0.0282$ ), with significant value dispersion ( $p = 0.0794$ ). A comparison between control mDA and grafted mDA neurons showed that this significant decrease in firing rate affected both regular and irregular grafted mDA neurons. Indeed, irregular grafted mDA neurons fired nearly three times less than irregular control mDA neurons ( $1.88 \pm 1.60$  Hz,  $n = 12$ ,  $CV = 0.85$  vs.  $4.94 \pm 2.17$  Hz,  $n = 12$ ,  $CV = 0.44$ ;  $p = 0.0008$ ), while regular grafted mDA neurons displayed a discharge frequency 40% lower than regular control mDA neurons ( $3.19 \pm 0.69$  Hz,  $n = 6$ ,  $CV = 0.2$  vs.  $5.26 \pm 2.31$  Hz,  $n = 8$ ,  $CV = 0.44$ ;  $p = 0.0418$ ). Finally, regarding the frequency value range for the irregular pattern in both control mDA and grafted mDA neurons, the distribution was similar

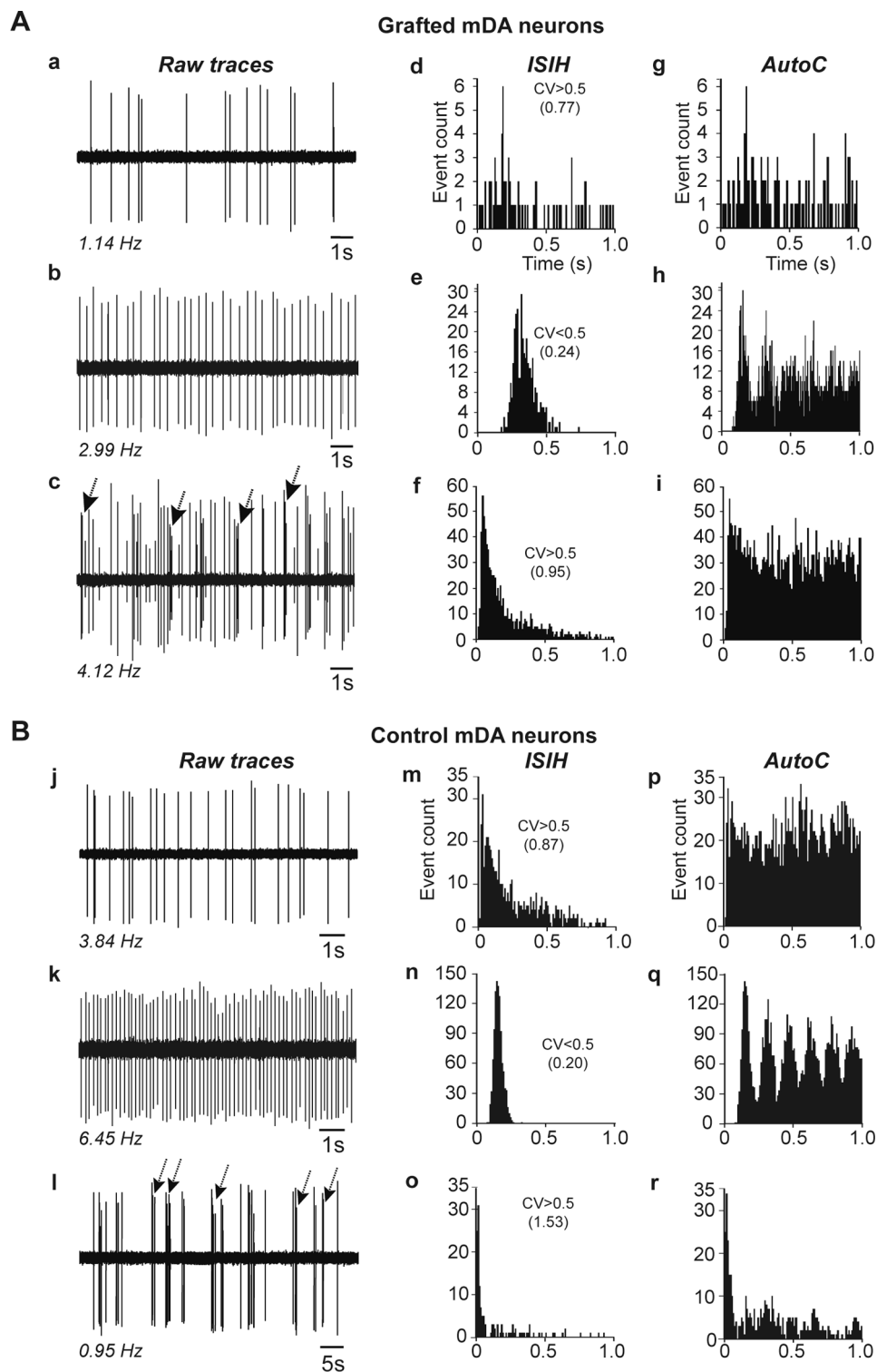


**Fig. 6** In vivo spontaneous electrophysiological profiles of grafted mDA and control mDA neurons. **(A, B)** Representative single-unit extracellular recordings of different spontaneous activity patterns and their correlated descriptive analyses in grafted mDA neurons **(A)** and control mDA neurons **(B)**. Discharge pattern examples (raw traces) recorded in different neurons exhibited irregular **(a and j)**, regular **(b and k)** and bursting mode **(c and l)**; Arrows indicated bursting episodes). For each recorded neuron, the distribution of time duration between spikes is displayed as ISIH (10 ms bin width / 1 s interval; see **d, e, f** and **m, n, o**) and AutoC (10 ms bin width / 1 s interval; see **g, h, i** and **p, q, r**) to determine the discharge mode and potential rhythmicity occurrence, respectively. Abbreviations: ISIH, interspike interval histogram; AutoC, autocorrelogram; CV, coefficient of variation



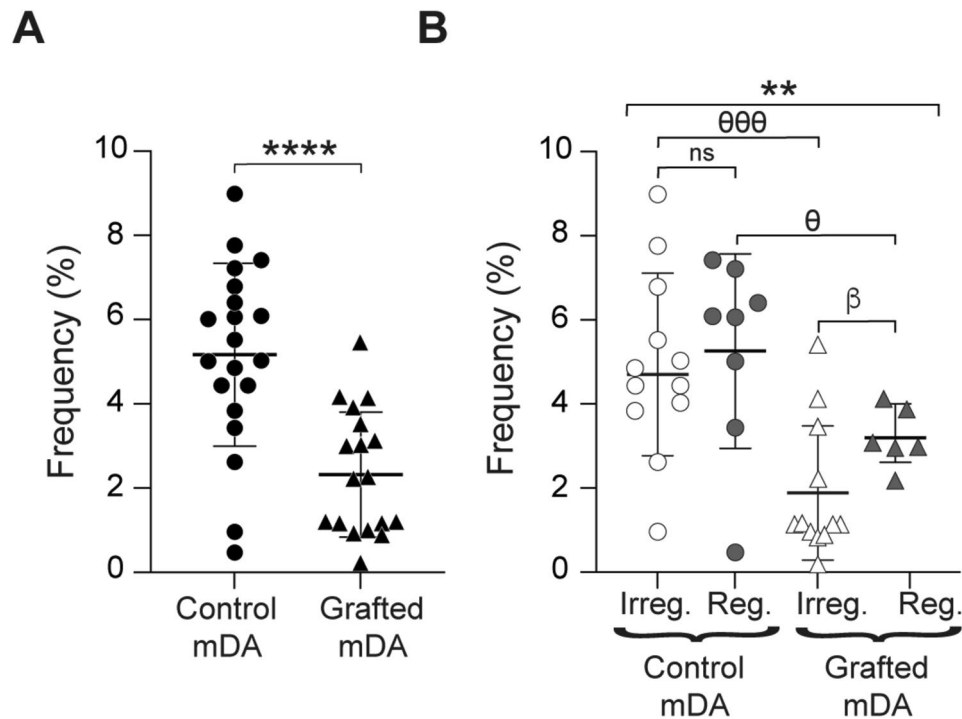


**Fig. 7** Frequencies of spontaneous electrophysiological activities of grafted mDA and control mDA neurons. **(A)** Comparison of mean rate frequency and value distribution between control mDA ( $n=20$ ) and grafted mDA ( $n=18$ ) neurons. An unpaired t-test showed a significant difference ( $p < 0.0001$  \*\*\*\*) between mean rate frequencies but a similar value distribution (F-test;  $F(\text{Df}_n, \text{Df}_d) = 2.142$  [17, 19];  $p = 0.1204$ ). **(B)** Analysis of discharge frequency related to firing patterns. Grafted mDA and control mDA populations were splitted into sub-populations depending on the discharge pattern: Irreg control mDA (white dots;  $n=12$ ), reg control mDA (grey dots;  $n=8$ ), irreg (white triangles;  $n=12$ ) and reg grafted mDA (grey triangles;  $n=6$ ). A one-way ANOVA comparison revealed that frequency was strongly influenced by patterns and experimental conditions ( $W(\text{Df}_n, \text{Df}_d) = 6.85(3, 17.68)$ ;  $p = 0.0029^{**}$ ). Pairwise analysis indicated grafted mDA neuron frequency and value distribution were dependent on the firing pattern (unpaired t-test ( $t, \text{df}$ ) = 2.414, 15.90;  $p = 0.0282^{\theta}$ ); value distribution  $F(\text{Df}_n, \text{Df}_d) = 5.268$  [5, 11];  $p = 0.0794$ ), in contrast to control mDA neurons (unpaired t-test ( $t, \text{df}$ ) = 0.313, 14.47;  $p = 0.76$ ; value distribution F-test;  $F(\text{Df}_n, \text{Df}_d) = 1.134$  [7, 11];  $p = 0.8173$ ). Both irregular and regular grafted mDA neurons exhibited a decrease in firing rate compared to control mDA neurons (Irreg neurons, unpaired t-test ( $t, \text{df}$ ) = 3.923, 20.21;  $p = 0.0008^{000}$ ; reg neurons, unpaired t-test ( $t, \text{df}$ ) = 2.389, 8.618;  $p = 0.0418^{\theta}$ ). Value distribution was similar in both irregular control mDA and grafted mDA neurons (F-test;  $F(\text{Df}_n, \text{Df}_d) = 1.847$  [11];  $p = 0.3236$ ), but more dispersed in regular control mDA neurons than in regular grafted mDA neurons (F-test;  $F(\text{Df}_n, \text{Df}_d) = 11.03$  [5, 7];  $p = 0.0177$ ). Abbreviations: Irreg, irregular pattern; Reg, regular pattern

( $p = 0.3236$ ), whereas for regular neurons, the distribution was significantly more dispersed in control mDA neurons compared to grafted mDA neurons ( $p = 0.0177$ ).

Then, we analyzed the distribution of different discharge patterns in both grafted mDA and control mDA populations. Statistical analysis showed a similar distribution between irregular and regular patterns, regardless of the dopaminergic population considered (Fig. 8A). During spontaneous discharge, some neurons exhibited bursty episodes superimposed on the main discharge pattern. 75% of control mDA neuronal population displayed bursty activity, while only 22% of grafted mDA neurons exhibited this high-frequency discharge mode (Fig. 8B). Depending on the discharge pattern and bursting mode, four neuronal subpopulations were distinguished: bursty irregular (1), bursty regular (2), non-bursty irregular (3) and non-bursty regular (4). The distribution of control mDA neurons was divided as follows: 55% bursty irregular, 20% bursty regular, 5% non-bursty irregular and 20%

non-bursty regular neurons. However, the grafted mDA neuronal population exhibited a significantly different distribution and a weaker capacity to evoke bursts. Specifically (1), all bursty grafted mDA neurons displayed an irregular pattern (22%) and (2) the remaining neurons were distributed as 45% irregular and 33% regular.

As previously demonstrated, some neurons generated transient episodes of high-frequency activity, termed bursts, composed of two to six consecutive spikes (Fig. 9). However, these bursting neurons exhibited a distinct bursting potential, which was evaluated using the percentage of spikes in bursts (SIB in Fig. 9A). Comparative analysis between both dopaminergic populations showed similar mean SIB values and similar distributions in control mDA ( $40.23 \pm 26.45\%$ ,  $n=15$ ;  $\text{CV} = 0.65$ ) and grafted mDA ( $25.69 \pm 12.35\%$ ,  $n=4$ ;  $\text{CV} = 0.48$ ) neurons. The SIB ranged from 11 to 89% for control mDA bursty neurons and from 11 to 41% for grafted mDA bursty neurons. We then arbitrarily graded neurons into three classes

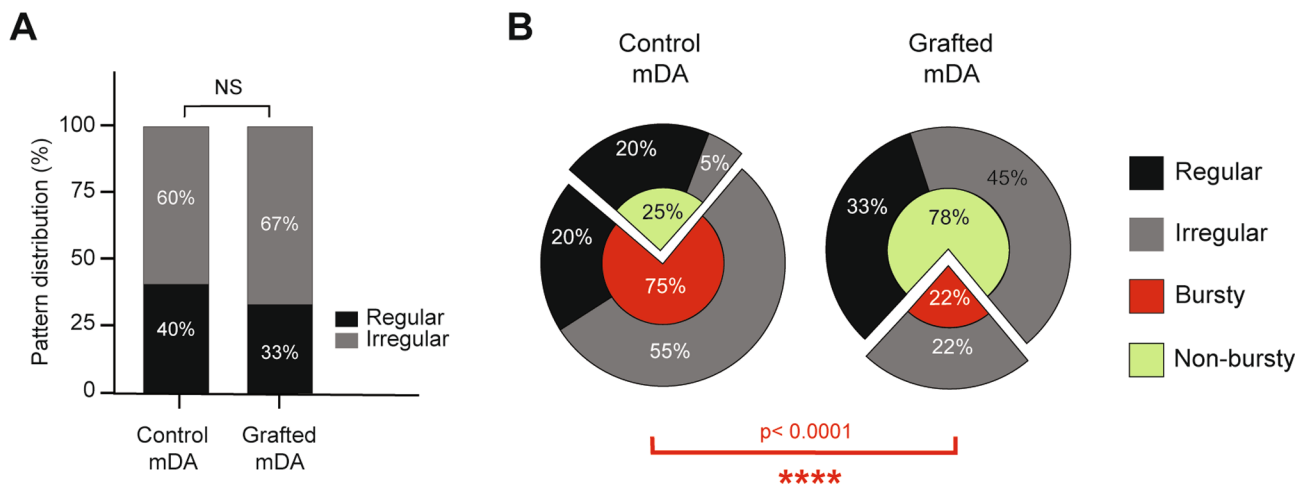


**Fig. 8** In vivo firing pattern repartition and bursty potential in control mDA and grafted mDA populations. **(A)** Distribution of firing regular (grey) / irregular (black) patterns. Comparative analysis showed similar repartition in both populations (control mDA  $n=20$ ; grafted mDA  $n=18$ ; Fisher test,  $p=0.3782$ ). **(B)** Relative distribution of bursting mode within irregular and regular discharge patterns in control mDA and grafted mDA neurons. In each dopaminergic population (i.e. control mDA and grafted mDA), the central circle represents the fraction of bursty (red) and non-bursty neurons (green). The peripheral circle displays the ratios of irregular (grey) and regular (black) discharge patterns. Comparative analysis of sub-population distribution between control mDA and grafted mDA neurons showed a differential distribution of neurons related to bursty mode (Chi-square test DF [3],  $P<0.0001$ )

depending on the SIB percentage (Table 1): low (below 20%), intermediate (21–50%) and highly bursty (above 50%). The grafted mDA bursty neurons did not perform better than intermediate SIB ( $33.89 \pm 10.56\%$ ,  $n=2$ ;  $CV=0.31$ ), while 35% of control mDA neurons exhibited a highly bursty potential ( $72.35 \pm 7.93\%$ ;  $n=7$ ;  $CV=0.17$ ).

We then examined the characteristics of these bursts. Similarly to bursty control mDA neurons, bursts of grafted mDA neurons were mainly composed with two to six consecutive spikes, firing with decreasing amplitude and increasing interspike intervals. Comparative analysis showed no difference in the average spike count between the two dopaminergic neuron populations (Fig. 9B: grafted mDA  $3.496 \pm 1.044$ ,  $n=4$ ,  $CV=0.29$ ; control mDA  $3.559 \pm 1.036$ ,  $n=15$ ,  $CV=0.29$ ). We observed that some bursty neurons could produce seven to twelve spikes within bursts, and these bursts were categorized as a single group (“up from 7”) for further burst data analysis. In grafted mDA neurons, the relative burst distribution based on the SIB number followed a similar linear trend to that observed in control mDA neurons (Fig. 9C). Thus, in both grafted mDA and control mDA neurons, bursts with 2 spikes represented the largest proportion (control mDA:  $44.07 \pm 19.53\%$ ; grafted mDA:  $33.80 \pm 30.20\%$ ), and as the number of spikes in bursts increased, the proportion of bursts decreased (Table 2).

As shown in Fig. 9D, grafted mDA bursty neurons displayed an intraburst frequency ( $24.31 \pm 7.142$  Hz,  $n=4$ ,  $CV=0.29$ ) in line with that of control mDA bursty neurons ( $28.66 \pm 5.131$  Hz,  $n=15$ ,  $CV=0.18$ ). These similar parameters between the two dopaminergic populations were further observed for the mean first interspike interval ( $Isi_1$ ) to start a burst (control mDA  $54.28 \pm 11.44$ ,

$n=15$ ,  $CV=0.21$  vs. grafted mDA  $44.29 \pm 11.06$ ,  $n=4$ ,  $CV=0.25$ ; Fig. 9E). Lastly, we studied the consecutive interspike intervals in bursts, as it has been widely described in the literature that bursts in dopaminergic neurons are also characterized by increasing consecutive ISIs intraburst during the burst. We thus determined 3 consecutive ISIs ( $Isi_1$ ,  $Isi_2$ ,  $Isi_3$ ) in bursts with four spikes (Fig. 9F). Comparative analysis showed a significant difference between ISIs in control mDA ( $p<0.0001$ ) and grafted mDA ( $p=0.0046$ ) neurons. However, although we observed an increase between the two consecutive ISIs in control mDA neurons ( $Isi_1 < Isi_2$ ;  $p<0.0001$ ;  $Isi_2 < Isi_3$ ;  $p<0.0024$ ), there was no difference between  $Isi_1$  vs.  $Isi_2$  and  $Isi_2$  vs.  $Isi_3$  in grafted mDA neurons.

## Discussion

### Intranigral versus intrastriatal transplantation

The intrastriatal grafting approach, which is currently used in clinical trials for PD, is limited by the fact that mDA neurons are implanted in the striatum, the target area, rather than the substantia nigra, where they are normally located. This ectopic localization of cells may affect the functionality of transplanted neurons due to the lack of appropriate host afferent regulation [14, 43]. Our group and the Björklund group, were the first to demonstrate that fetal mDA neurons grafted into the substantia nigra in animal models of PD can form axonal projections to the striatum, resulting in increased dopamine levels and improvements in motor deficits [12, 44]. Furthermore, we showed that intranigral grafts promoted better survival of dopaminergic neurons and led to recovery of fine motor skills and normalized corticostriatal responses [45]. Neuroanatomical and functional

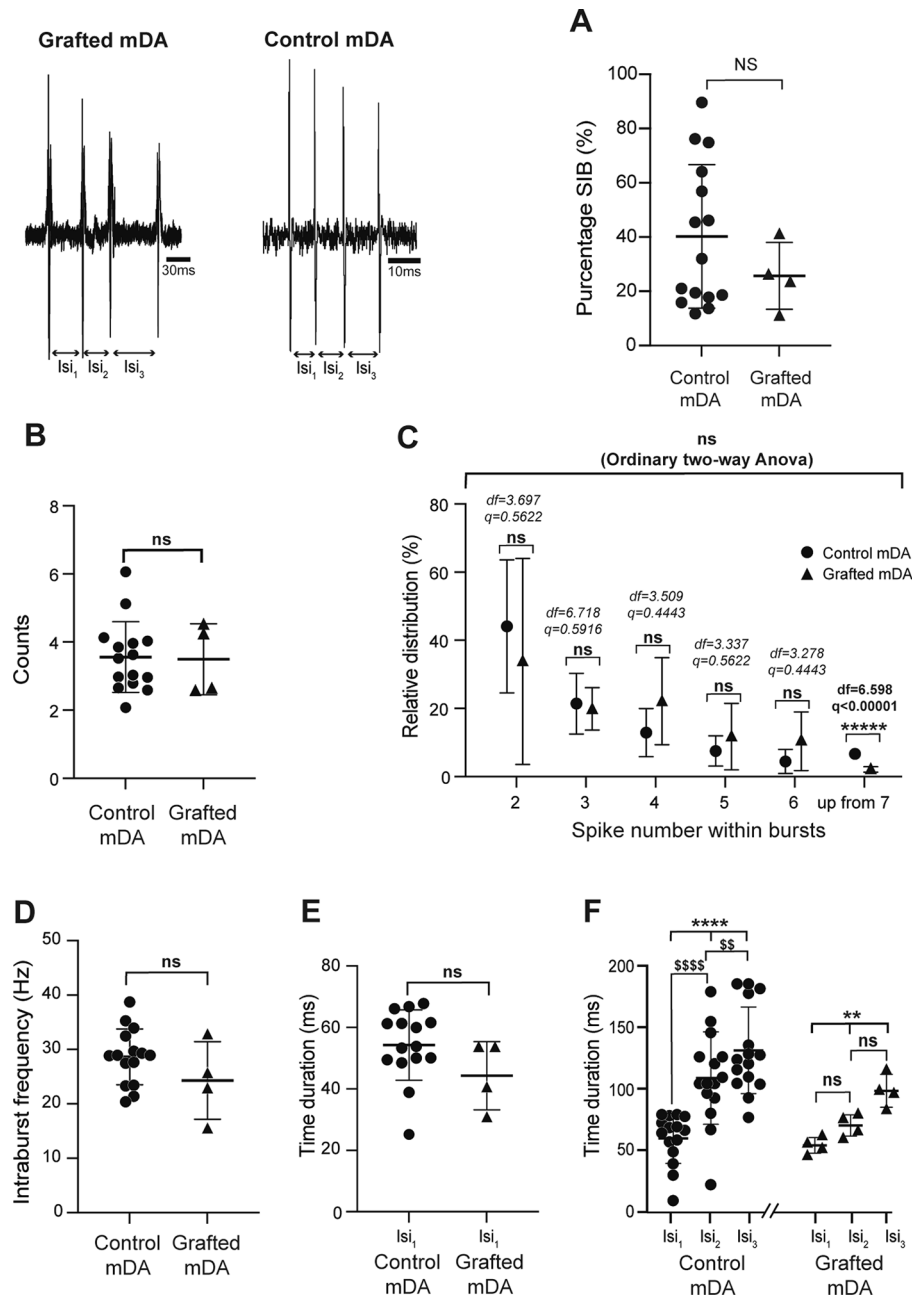


**Fig. 9** Properties of bursting activity in control mDA and grafted mDA neurons: **(A)** Spikes in burst (SIB) percentage. Statistical analyses were performed using the Mann-Whitney test ( $p=0.469$ ) and the Fisher test for value distribution ( $F(Df_n, Df_d)=4.584$  [3, 14];  $p=0.235$ ). Each plot represents a single neuron. **(B)** Mean spike number in bursts. Each plot represents the average spike number in bursts from 150–180 s of spontaneous activity in a single neuron. Statistical analysis was performed using the Mann-Whitney test ( $p=0.961$ ). **(C)** Relative occurrence of bursts depending on spike number within burst. Bursts were categorised into 6 groups based on spike number (2,3,4,5,6 and  $\geq 7$  spikes), with their distribution determined relative to the total number of bursts. Each plot represents the average distribution from the considered neurons in each population. Statistical comparison was performed using a 2-way ANOVA ( $F$  [5, 107] = 4.078;  $p=0.998$ ). Only bursts with more than 7 spikes showed differing proportions between the dopaminergic populations (multiple unpaired t-tests;  $df=6.598$ ,  $q<0.00001$ ). **(D)** Mean intraburst frequency. Statistical analysis was performed using the Mann-Whitney test ( $p=0.262$ ). **(E)** First ISI (Isi<sub>1</sub>) to start a burst. Each plot represents the Isi<sub>1</sub> in burst averages, calculated from all bursts in a single neuron. Statistical analysis was performed using a Mann-Whitney test ( $p=0.152$ ). **(F)** Consecutive ISIs in bursts (Isi<sub>1</sub>, Isi<sub>2</sub>, Isi<sub>3</sub>) from bursts within 4 spikes. Isi increment within the burst course was shown in control mDA (paired one-way ANOVA test:  $F(Df_d, Df_d)=F(1.679, 23.50)=41.03$ ;  $p<0.0001$ ) and in grafted mDA (non-parametric paired Friedman test,  $p=0.004$ ) neurons. In control mDA neurons, paired t-test showed significant increases in consecutive Isis over time (Isi<sub>1</sub> < Isi<sub>2</sub>: t-test(t, df)=(5.551, 14),  $n=15$ ,  $p<0.0001$ ; Isi<sub>2</sub> < Isi<sub>3</sub>: t-test(t, df)=(3.705, 14),  $n=15$ ,  $p<0.002$ ) but not in grafted mDA neurons (wilcoxon matched-pairs signed rank test). Each plot represents the average Isi between 2 spikes in a burst from a single neuron. Scatterplots and analyses were performed on 15 control mDA and 4 grafted mDA bursty neurons. All data are means  $\pm$  SD. Abbreviations: ISI, interspike interval; SIB, spike in burst

**Table 1** Bursting potential

SIB	Control mDA	grafted mDA
Mean ± SD, n (CV)		
All neurons <sup>1</sup>	40.23 ± 26.45% n = 15 (CV = 0.65)	25.69 ± 12.35% <sup>ns</sup> n = 4 (CV = 0.48)
Low (≥ 20%)	16.88 ± 3.29% n = 5 (CV = 0.19)	17.50 ± 8.82% n = 2 (CV = 0.50)
Intermediate (21–50%)	41.20 ± 7.93% n = 3 (CV = 0.19)	33.89 ± 10.56% n = 2 (CV = 0.31)
Highly (> 50%)	72.35 ± 12.51% n = 7 (CV = 0.17)	None

Bursting potential was assessed using the percentage of spikes in burst (SIB). Classification was performed based on their burst potential, defined by the SIB percentage obtained from 150–180 s of spontaneous activity. Three clusters were defined: low (below 20%), intermediate (21 to 50%) and highly bursty (above 50%). Bursting mode was considered for SIB values over a 1% threshold. Data were expressed as mean ± SD, with n representing the number of bursty neurons; <sup>ns</sup> indicated not significant difference. <sup>1</sup>: Mean analysis and value dispersion between the two dopaminergic populations were performed using an unpaired t-test with Welch's correction (t, df = 1.58, 11.22; p = 0.142) and an F test (F, DFn, Dfd = 4.584, 14, 3; p = 0.236), respectively

**Table 2** Burst repartition depending on Spike number in burst

Spike number in burst	Control mDA (n = 15)	grafted mDA (n = 4)
2	44.07 ± 19.53%	33.80 ± 30.20%
3	21.40 ± 8.89%	19.86 ± 6.23%
4	12.89 ± 7.08%	22.13 ± 12.74%
5	7.53 ± 4.43%	11.74 ± 9.76%
6	4.43 ± 3.56%	10.36 ± 8.62%
7+	6.96 ± 1.10%	2.08 ± 0.79%

The percentage burst values were plotted against the number of spikes constituting them. These data corresponded to the values shown in the scatterplot in Fig. 9C

restoration of the degenerated nigrostriatal pathway was later confirmed using mDA neurons obtained from human pluripotent stem cells grafted into the into the SN in animal models of PD [46, 47, 66, 67]. Overall, these findings demonstrate the capacity of intranigral dopaminergic neuron grafts to restore the damaged nigrostriatal pathway in animal models of PD.

However, to date, the in vivo electrophysiological functionality of dopaminergic neurons grafted into the SNpc has not been demonstrated. This present study represents the first preclinical report on the in vivo electrophysiological activity of intranigral-grafted mDA neurons in an animal model of PD.

**Dopaminergic-like hallmarks of grafted mDA neurons**  
**The Spike waveform**

In vivo recordings of grafted mDA neurons revealed characteristics similar to those described in nigral mDA neurons from the control group and in previous studies relating to mesencephalic DA neurons in the SNpc or ventral tegmental area [32, 68, 69], as well as in intranigral murine fetal mesencephalic transplants [31]. The first feature concerned the typical action potential waveform, which was distinguished by (1) bi-phasic or tri-phasic

patterns (2), a notch in the depolarizing phase (3), a large repolarizing phase, and (4) a clearly long duration (over 2 ms). This latter point is a major factor for identification during electrophysiological recordings, as it distinguishes mDA neurons from others neurons with similar discharge patterns but much shorter spike durations, such as GABAergic neurons [32, 34]. In our study, the mean spike duration of grafted mDA neurons was consistent with that of control mDA neurons. Additionally, we focused on the initial phase duration (IT), which has also been described as a distinctive and well-preserved criterion of dopaminergic identity [60, 61]. Similarly, grafted mDA neurons exhibited IT values comparable to those of control mDA neurons in the SNpc.

While the action potentials of grafted mDA neurons display similar components to those of in vivo recorded control mDA neurons in mice, what about mDA neurons in human *substantia nigra*?

Sparse clinical studies have performed electrophysiological recordings of the dorsal *substantia nigra* in patients undergoing deep brain stimulation (DBS) for PD [65, 66]. These clinical data showed that the spike half-maximal duration (HS) of human mDA neurons ranged from 0.81 to 1.6 ms, which is in line with the HS value dispersion of grafted mDA neurons (0.75 to 1.91 ms) that we observed. Thus, in our study, grafted mDA neurons generated in vitro display action potentials with comparable properties to nigral mesencephalic dopaminergic neurons in the human brain. This suggests that grafted mDA neurons possess the appropriate membrane channel receptors and molecular tools to produce spikes with a dopaminergic-like phenotype.

**Diversity of firing dopaminergic-like patterns**

We showed that control mDA and grafted mDA neurons displayed single-spike firing in patterned activity, either regular or irregular. Both patterns were distributed equally in control mDA and grafted mDA neurons. While we described a regular discharge pattern in both grafted mDA and control mDA neurons, this firing pattern has been poorly described in in vivo anesthetized animals [32, 70]. Indeed, it is believed to be specific to in vivo awake animal studies during driven behaviors [71, 72], but also to ex vivo conditions with the loss of synaptic inputs and the involvement of intrinsic rhythmic mechanisms [73, 74]. Extensively studied in ex vivo brain slices, this rhythmic autogenic activity is triggered by membrane voltage oscillations, generating a unique action potential at each oscillation peak. The action potential genesis is induced by a slow inward voltage-dependent current that induces membrane depolarisation to reach spike threshold. The spike is regulated by different ionic conductances, but the most remarkable is a large activation of the outward K(Ca<sup>2+</sup>) current, inducing significant



post-hyperpolarisation after massive  $\text{Ca}^{2+}$  entry resulting from both the spike-related conductances and oscillatory membrane potential [75, 76]. This endogenous discharge pattern is believed to play an important functional role by synchronising neuronal activity during the establishment of a behavior [77, 78]. In our study, the presence of a regular discharge pattern in both dopaminergic populations could be related to experimental conditions, particularly the impact of isoflurane anaesthesia. Indeed, a previous study demonstrated that isoflurane modifies the excitability of nigral dopaminergic neurons in rat midbrain slices by inducing membrane depolarisation and increasing discharge frequency [79]. The excitability of nigral dopaminergic neurons is known to be partially dependent on A-type K channels, which play a key role in controlling the endogenous pacemaker [80], and its increase could therefore be induced by a temporal shift in A-type K channel inactivation in vivo in rats [81]. These reports suggest that grafted mDA neurons provide the required molecular machinery for sustained endogenous rhythm.

Human iPSC-derived mDA neurons could also produce a stable, irregular spontaneous firing pattern, similarly to that of control mDA neurons. This irregular mode is characterized by a single-spike discharge driven by analogous membrane mechanisms described for pacemaker-type discharge (see above) and is strongly regulated by  $\text{IK}(\text{Ca}^{2+})$  conductance [82]. However, the irregular single-spike activity would also be regulated by a strongly inhibitory GABAergic input coming from the globus pallidus (GP) and *substantia nigra pars reticulata* (SNpr) [83], inhibiting the bursting activity of dopaminergic neurons, inducing pauses and silence, and finally supporting the shift between regular and irregular patterns [35, 84]. Collectively, these data suggest that irregular firing is probably associated with both slow intrinsic depolarisation and, mainly, with variations in  $\text{Ca}^{2+}$  influx, and a GABAergic modulation.

In control mDA neurons, we showed both single-spike discharges (tonic and irregular) could produce bursts. Similar bursty activity is found in a few grafted mDA neurons but concerns only irregular neurons.

Although few grafted mDA neurons displayed bursts, our grafted neurons were competent to generate episodes of transient high-frequency bursting superimposed on single action potential discharge. This observation is significant because it supports the expectation that grafted mDA neurons received functional afferents. Indeed, although the mechanisms underlying bursts are poorly understood, the best assumption about dopaminergic burst genesis and modulation is underpinned by at least two mechanisms: down-regulation of  $\text{K}(\text{Ca}^{2+})$  current [85, 86] and glutamatergic activation of NMDA/AMPA/kainate receptors located on the dendritic arborisation of dopaminergic neurons [87, 88]. In physiological

conditions, the glutamatergic inputs come mainly from the *subthalamic nucleus* (STN), the somatosensory/motor cortices, the *pedunculopontine tegmental nucleus* (PPTg), or the lateral hypothalamus [89]. Some of these (STN and PPTg) are effective at increasing the intensity of in vivo bursting activity (i.e. duration and frequency of bursts), but also at inducing bursts in dopaminergic cells with an initial non-bursty irregular discharge pattern [82, 90]. Moreover, striatal GABAergic afferents were shown to play a key role in bursting activity since they are the main inhibitory source of PPTg [84, 91]. In intranigral graft conditions, several studies using rabies virus tracing have reported various afferences, including glutamatergic excitatory inputs from mainly motor and prefrontal and sensorimotor cortical regions, but also from other cerebral areas (hypothalamus, bed nucleus of the stria terminalis, central amygdala, ventral pallidum, dorsal raphe nuclei, pontine reticular nucleus) [48, 49, 92]. Considering bursts are excitatory input-dependent, and we previously showed that no glutamatergic neurons derived from hiPSCs were present in the graft [46], our results strongly suggest that grafted mDA neurons receive functional glutamatergic excitatory inputs from the host, responsible for inducing bursty activities.

In addition, we showed that the proportion of grafted mDA neurons displaying bursting mode was three folds lower than that of control mDA neurons in control mouse. This suggests that grafted mDA neurons could receive fewer excitatory modulatory afferents required for bursty activity and/or could be under strong tonic GABAergic inhibition. In this latter hypothesis, this inhibitory modulation could come from the main well-known structures regulating the nigral mDA neurons, namely SNpr, globus pallidus and striatum. However, we cannot exclude the possibility that this tonic inhibition could also be reinforced by a local network in the graft. Indeed, we showed in our previous study, and confirmed here, that the graft is composed not only of mDA neurons but also of other cells, including about 10% GABAergic neurons derived from hiPSCs [46]. Furthermore, electrophysiological data from non-dopaminergic neurons (data not shown) exhibited typical profiles of inhibitory interneurons, specifically GABAergic neurons, characterized by high-frequency firing (above 20 Hz) and short spike duration (below 1 ms). However, since these non-dopaminergic neurons were not injected with neurobiotin, we cannot confirm their GABAergic identity or determine whether they have a human origin.

This idea of the grafted mDA neurons being modulated by a strong inhibitory tonic control might be supported by another observation. Indeed, we showed that irregular grafted mDA neurons displayed weaker discharge frequencies than regular grafted mDA neurons (a feature not observed in nigral mDA neurons). In addition, rabies

tracings in grafted hESC-derived mDANeurons reported that these grafted mDA received more inhibitory and fewer excitatory inputs [49]. Therefore, this could support the hypothesis that the decreased frequency of irregular grafted mDA neurons could be the consequence of strong GABAergic input reinforced by GABAergic local neurons in a context of weak excitatory control.

Finally, we noticed that while both irregular and regular control mDA neurons can express bursty activity, only irregular grafted mDA neurons exhibited bursts. This discrepancy could be due to different functional factors. First, we might consider whether the number and/or density of glutamatergic inputs are insufficient to provide the required excitatory tone to induce bursts. Indeed, studies have demonstrated that glutamatergic afferents from the STN, prefrontal cortex, raphe nuclei, and PPTg are critical for sustaining an appropriate excitatory tone and then facilitating burst generation [93, 94]. Conversely, it has also been shown that, because glutamatergic excitatory input from the STN is too extensive, membrane depolarisation is inhibited, preventing bursts [95]. This functional hypothesis could result from overinhibition of GABAergic inputs from the GP/ PPTg to nigral dopaminergic neurons.

#### **Low firing frequency of grafted mDA neurons derived from hiPSCs neurons: a hallmark of human neurons?**

Regardless of the firing pattern, the discharge frequencies of grafted mDA and control mDA neurons were below 10 Hz. These data align with previous *in vivo* studies that reported different patterned activities in anesthetized [32, 34, 82] and awake [34, 35] animals. In our study, the comparative analysis shows that the discharge frequency of grafted mDA neurons was twofold lower than that of control mDA neurons. This finding is consistent with numerous *in vitro* studies using mDA neurons derived from various hiPSC lines, and reporting similar frequency ranges [19–21].

This finding raises questions about the neuronal properties associated with species origin, particularly regarding human nigral mDA neurons. *Ex vivo* electrophysiological studies offer valuable insights into functional specificities of human neurons. Indeed, studies on human cortical pyramidal neurons have demonstrated unique intrinsic and membrane properties that contribute to greater synaptic plasticity but reduced intrinsic neuronal excitability compared to the neuronal excitability of mouse cortical pyramidal neurons [96, 97]. These differences have been linked to the *LRRC37B* gene, which is exclusive to hominids. In experiments involving *LRRC37B*-positive mouse cortical pyramidal neurons, reduced excitability was observed, mirroring the characteristics of human neurons. In this context, we propose that the reduced discharge frequency in grafted mDA

neurons derived from human iPSC may reflect a lower intrinsic excitability of human neurons compared to murine neurons. This is particularly significant, as neuronal excitability plays a crucial role in generating endogenous firing or for responding to synaptic inputs [98, 99]. This hypothesis is further supported by observations of regular firing patterns originating from intrinsic oscillatory properties, even in the absence of functional synaptic connections [73, 100].

#### **The long-term neuronal maturation of grafted mDA neurons**

An important aspect following transplantation is the functional maturation of the grafted neurons. This issue can be assessed through the relative firing rate distribution, which reflects the functional heterogeneity of the grafted mDA neuronal population. Although statistical analysis of firing rate distributions did not reveal a significant difference between the two dopaminergic populations (i.e. control mDA and grafted mDA neurons), the frequency distribution within the grafted mDA population tended to be less heterogeneous. This functional heterogeneity of mesencephalic dopaminergic neurons is well-documented in both rodents and primates. This diversity is influenced by functional maturation, which is linked to intrinsic cellular properties (e.g. synaptic plasticity; gene divergence; molecular characteristics etc.) and integration within the neuronal networks (e.g. modulatory inputs, efferent projections to target regions etc...) [101, 102]. For instance, *in vivo* rodent studies have highlighted significant functional diversity among nigral dopaminergic neurons along the medio-lateral axis of the SNpc. These studies revealed variations in both electrical properties (e.g. oscillatory firing rates, occurrence of bursty firing mode) and network properties (e.g. differing mean discharge frequencies) in [100, 102]. This evidence suggests that the observed reduction in heterogeneity within the grafted mDA neuronal population could reflect an incomplete or ongoing maturation process. Further investigations are needed to understand whether this limited functional diversity impacts the overall efficacy of mDA grafts in restoring dopaminergic functionality.

In our current work, the relative functional homogeneity of grafted mDA neurons within the graft could be attributed to differential maturation associated with their human origin. Between eight and twelve MPT, we previously demonstrated that approximately half of grafted cells were mature (HuNu<sup>+</sup>/NeuN<sup>+</sup>), with one-third of mature neurons exhibiting a dopaminergic phenotype (HuNu<sup>+</sup>/NeuN<sup>+</sup>/TH<sup>+</sup>) [46]. Meanwhile, one year after transplantation, 18% of grafted neurons remained immature, as evidenced by the expression of DCX, a marker of immature neurons.

Furthermore, several studies have shown that neurons derived from hESCs or hiPSCs transplanted into the mouse brain require a prolonged maturation period [51, 103]. This could explain the limited functional variability and heterogeneity observed between grafted mDA and control mDA neurons, potentially reflecting the intrinsic characteristics of human-derived cells.

When comparing neurogenesis in humans and mice, the maturation processes differ significantly in both temporality and complexity [104]: while neurogenesis begins early during embryonic development in most species, the complete maturation of neuronal circuitry extends beyond birth into adolescence and even adulthood in humans [105, 106]. In contrast, neuronal maturation in mice is typically completed within the first few weeks after birth [107].

## Conclusion

Our findings confirmed our previous results showing that mDA derived hiPSC progenitors grafted into the SNpc in a mouse model of PD, differentiated into mature mDA neurons, restored the degenerated nigrostriatal pathway, and induced motor recovery. In this study, we further showed that intranigral grafted mDA neurons exhibited intrinsic electrophysiological properties consistent with a dopaminergic-like phenotype, as well functional attributes suggesting excitatory and inhibitory interactions with other cerebral regions known to modulate nigral mesencephalic dopaminergic neurons. Several studies have reported that intranigral grafts of mDA neurons derived from hESCs received host-specific afferents, matching those of native mDA neurons. Our electrophysiological results suggest that host afferent inputs received by mDA intranigral grafts are functional.

Overall, our findings, along with results from other groups, demonstrate the ability of intranigral mDA neuron grafts to repair the damaged nigrostriatal pathway in a more physiological way than intra-striatal grafts. This promising approach needs further investigation to improve the efficacy of transplantation and its potential for future clinical application in patients.

## Abbreviations

AccN	Accumbens nucleus
AP	Antero-posterior
AutoC	Autocorrelogram
CPu	Caudal putamen
CV	Coefficient of variation
DBS	Deep brain stimulation
dStr	dorsal striatum
DV	Dorso-ventral
FP	Floor plate
Fv-mDA	Fetal ventral mesencephalic tissue-derived mesencephalic dopaminergic
GAD	Glutamate decarboxylase
GP	Globus pallidus
(h)ESCs	(human) Embryonic stem cells

(h)ESC-derived mDA	(human) Embryonic stem cell-derived mesencephalic dopaminergic
(h)IPSCs	(human) Induced pluripotent stem cells
hiPSC-derived GABA	human induced pluripotent stem cell-derived GABAergic
hiPSC-derived mDA	human induced pluripotent stem cell-derived mesencephalic dopaminergic
HS	Half-maximal spike duration
HuNu	Human nuclear
I.P.	Intraperitoneal
IS	Initial spike duration
ISI(H)	Interspike interval (histogram)
mDA	mesencephalic dopaminergic
MFB	Medial forebrain bundle
ML	Medio-lateral
MPT	Month post transplantation
PD	Parkinson's disease
PBS	Phosphate buffer solution
PSCs	Pluripotent stem cells
PFA	Paraformaldehyde
PPTg	Pedunculopontine tegmental nucleus
RT	Room temperature
SD	Standard deviation
SIB	Spike intraburst
SN	Substantia nigra
SNpc	Substantia nigra pars compacta
SNpr	Substantia nigra pars reticulata
STN	Subthalamic nucleus
TH	Tyroxine hydroxylase
TS	Total spike duration
VTA	Ventral tegmental area
6-OHDA	6 hydroxydopamine

## Acknowledgements

Acknowledgements to staff of PREBIOS platform (zootechnical facility for animal accommodation and caring) and ImageUP platform for imaging acquisition.

## Author contributions

BB conducted the electrophysiological recordings, the tissue processing, the immunohistochemical processes, the data analysis, and wrote the manuscript. SB engineered and developed the hiPSC line and hiPSC-derived mDA precursors. He also performed the experimental group allocations and participated to immunohistochemical data analysis, 6-OHDA injections and transplantation processes. MLB participated in the development of hiPSC line and hiPSC-derived mDA progenitors, and their sustaining. AG conducted the scientific project, performed 6-OHDA injections and transplantation processes. She also participated in writing the manuscript. All authors read and approved the final manuscript.

## Funding

This work was funding by grants from the Fondation de France (engt no 66517), the Fondation pour la Recherche Médicale (Victor and Erminia Mescler Price to Afsaneh GAILLARD), the European Regional Development Fund (FEDER-CPER, P-2020-BAFE-93, PC-2018-4040510), and the Nouvelle-Aquitaine region.

## Data availability

All data used and analysed in this study are fully available upon reasonable request. The authors declare that they have not use AI-generated work in this manuscript.

## Declarations

### Ethics approval and consent to participate

Experimental referenced procedures are performed in accordance with European legislative, administrative, and statutory authorities for animal experimentation (EU/Directive/2010/63 of the European Parliament and Council) and according to the guidelines of the Declaration of Helsinki. They were approved by ethics regional committee (N°84 COMETHEA Poitou-Charentes) and referenced under file number APAFIS#2019060311226483v2

(Project title: Reconstruction of damaged circuits by human stem cell transplantation in Parkinson's disease / Date of approval 09/03/2019). All efforts are made to reduce animal number and their suffering.

### Consent to publication

The human fibroblasts are sourced from the CliniSciences Company and are derived from human samples anonymously collected from donor biopsy. CliniSciences has authorisation for the importation and distribution of elements derived from the human body (French Ministry in charge of research, AC-2018-3168 and IE-2018-982) to their transfer for scientific purposes (Article L. 1243-3 and L. 12434 of the French Public Health Code - transposition of European Directive 2004/23/EC of 31 March 2004- ). Furthermore, CliniSciences Company confirms that all elements derived from the human body are sourced from donors who signed an informed consent form.

### Competing interests

the authors declare no interest conflicts regarding the publication of this paper.

### Author details

<sup>1</sup>Laboratoire des neurosciences expérimentales et cliniques (LNEC), Université de Poitiers– INSERM 1084, Poitiers Cedex 9 86073, France

<sup>2</sup>Centre hospitalier universitaire (CHU) de Poitiers, Poitiers 86021, France

Received: 17 August 2024 / Accepted: 15 April 2025

Published online: 09 May 2025

### References

1. Fearnley JM, Lees AJ. Ageing and Parkinson's disease: substantia nigra regional selectivity. *Brain*. 1991;114(5):2283–301.
2. Riederer P, Wuketich S. Time course of nigrostriatal degeneration in Parkinson's disease: A detailed study of influential factors in human brain amine analysis. *J Neural Transm*. 1976;38(3–4):277–301.
3. Lloyd K, Hornykiewicz O. Parkinson's disease: activity of L-Dopa decarboxylase in discrete brain regions. *Science*. 1970;170(3963):1212–3.
4. Parkkinen L, O'Sullivan SS, Collins C, Petrie A, Holton JL, Revesz T, et al. Disentangling the relationship between lewy bodies and nigral neuronal loss in Parkinson's disease. *J Park Dis*. 2011;1(3):277–86.
5. Gibb WR, Lees AJ. The relevance of the lewy body to the pathogenesis of idiopathic Parkinson's disease. *J Neurol Neurosurg Psychiatry*. 1988;51(6):745–52.
6. Nishino H. Intracerebral grafting of catecholamine producing cells and reconstruction of disturbed brain function. *Neurosci Res*. 1993;16(3):157–72.
7. Björklund A, Stenevi U. Reconstruction of the nigrostriatal dopamine pathway by intracerebral nigral transplants. *Brain Res*. 1979;177(3):555–60.
8. Dunnett SB. Functional repair of striatal systems by neural transplants: evidence for circuit reconstruction. *Behav Brain Res*. 1995;66(1):133–42.
9. Schmidt RH, Ingvar M, Lindvall O, Stenevi U, Björklund A. Functional activity of substantia nigra grafts reinnervating the striatum: neurotransmitter metabolism and [14 C]2-Deoxy-d-glucose autoradiography. *J Neurochem*. 1982;38(3):737–48.
10. Thompson LH, Parish CL. Transplantation of Fetal Midbrain Dopamine Progenitors into a Rodent Model of Parkinson's Disease. In: Reynolds BA, Deleyrolle LP, editors. *Neural Progenitor Cells* [Internet]. Totowa, NJ: Humana Press; 2013 [cited 2023 Feb 23]. pp. 169–80. (Methods in Molecular Biology; vol. 1059). Available from: [https://link.springer.com/https://doi.org/10.1007/978-1-62703-574-3\\_15](https://link.springer.com/https://doi.org/10.1007/978-1-62703-574-3_15)
11. Björklund A, Dunnett SB, Stenevi U, Lewis ME, Iversen SD. Reinnervation of the denervated striatum by substantia nigra transplants: functional consequences as revealed by Pharmacological and sensorimotor testing. *Brain Res*. 1980;199(2):307–33.
12. Gaillard A, Decressac M, Frappé I, Fernagut PO, Prestoz L, Besnard S, et al. Anatomical and functional reconstruction of the nigrostriatal pathway by intranigral transplants. *Neurobiol Dis*. 2009;35(3):477–88.
13. Kirkeby A, Grealish S, Wolf DA, Nelder J, Wood J, Lundblad M, et al. Generation of regionally specified neural progenitors and functional neurons from human embryonic stem cells under defined conditions. *Cell Rep*. 2012;1(6):703–14.
14. Gaillard A, Jaber M. Rewiring the brain with cell transplantation in Parkinson's disease. *Trends Neurosci*. 2011;34(3):124–33.
15. Song T, Chen G, Wang Y, Mao G, Wang Y, Bai H. Chemically defined sequential culture media for TH+ cell derivation from human embryonic stem cells. *Mol Hum Reprod*. 2008;14(11):619–25.
16. Takahashi K, Yamanaka S. Induction of pluripotent stem cells from mouse embryonic and adult fibroblast cultures by defined factors. *Cell*. 2006;126(4):663–76.
17. Takahashi K, Tanabe K, Ohnuki M, Narita M, Ichisaka T, Tomoda K, et al. Induction of pluripotent stem cells from adult human fibroblasts by defined factors. *Cell*. 2007;131(5):861–72.
18. Park IH, Zhao R, West JA, Yabuuchi A, Huo H, Ince TA, et al. Reprogramming of human somatic cells to pluripotency with defined factors. *Nature*. 2008;451(7175):141–6.
19. Doi D, Magotani H, Kikuchi T, Ikeda M, Hiramatsu S, Yoshida K, et al. Pre-clinical study of induced pluripotent stem cell-derived dopaminergic progenitor cells for Parkinson's disease. *Nat Commun*. 2020;11(1):3369.
20. Song B, Cha Y, Ko S, Jeon J, Lee N, Seo H, et al. Human autologous iPSC-derived dopaminergic progenitors restore motor function in Parkinson's disease models. *J Clin Invest*. 2020;130(2):904–20.
21. Kikuchi T, Morizane A, Doi D, Magotani H, Onoe H, Hayashi T, et al. Human iPSC cell-derived dopaminergic neurons function in a primate Parkinson's disease model. *Nature*. 2017;548(7669):592–6.
22. Sørensen AT, Thompson L, Kirik D, Björklund A, Lindvall O, Kokaia M. Functional properties and synaptic integration of genetically labelled dopaminergic neurons in intrastriatal grafts. *Eur J Neurosci*. 2005;21(10):2793–9.
23. Steinbeck JA, Choi SJ, Mrejeru A, Ganat Y, Deisseroth K, Sulzer D, et al. Optogenetics enables functional analysis of human embryonic stem cell-derived grafts in a Parkinson's disease model. *Nat Biotechnol*. 2015;33(2):204–9.
24. Uchida K, Momiyama T, Okano H, Yuzaki M, Koizumi A, Mine Y, et al. Potential functional neural repair with grafted neural stem cells of early embryonic neuroepithelial origin. *Neurosci Res*. 2005;52(3):276–86.
25. Zheng X, Han D, Liu W, Wang X, Pan N, Wang Y, et al. Human iPSC-derived midbrain organoids functionally integrate into striatum circuits and restore motor function in a mouse model of Parkinson's disease. *Theranostics*. 2023;13(8):2673–92.
26. Hills R, Mossman JA, Bratt-Leal AM, Tran H, Williams RM, Stouffer DG, et al. Neurite outgrowth and gene expression profile correlate with efficacy of human induced pluripotent stem Cell-Derived dopamine neuron grafts. *Stem Cells Dev*. 2023;32(13–14):387–97.
27. Tønnesen J, Parish CL, Sørensen AT, Andersson A, Lundberg C, Deisseroth K et al. Functional Integration of Grafted Neural Stem Cell-Derived Dopaminergic Neurons Monitored by Optogenetics in an In Vitro Parkinson Model. Mattson M, editor. *PLoS ONE*. 2011;6(3):e17560.
28. Strömberg I, van Horne C, Bygdeman M, Weiner N, Gerhardt GA. Function of intraventricular human mesencephalic xenografts in immunosuppressed rats: an electrophysiological and neurochemical analysis. *Exp Neurol*. 1991;112(2):140–52.
29. Fisher LJ, Young SJ, Tepper JM, Groves PM, Gage FH. Electrophysiological characteristics of cells within mesencephalon suspension grafts. *Neuroscience*. 1991;40(1):109–22.
30. Arbutnot G, Dunnett S, MacLeod N. Electrophysiological properties of single units in dopamine-rich mesencephalic transplants in rat brain. *Neurosci Lett*. 1985;57(2):205–10.
31. Besnard S, Decressac M, Denise P. In-vivo deep brain recordings of intranigral grafted cells in a mouse model of Parkinson's disease. *NeuroReport*. 2010;21(7):485–9.
32. Sanghera MK, Trulsson ME, German DC. Electrophysiological properties of mouse dopamine neurons: in vivo and in vitro studies. *Neuroscience*. 1984;12(3):793–801.
33. Saitoh K, Isa T, Takakusaki K. Nigral GABAergic Inhibition upon mesencephalic dopaminergic cell groups in rats. *Eur J Neurosci*. 2004;19(9):2399–409.
34. Aebischer P, Schultz W. The activity of Pars compacta neurons of the monkey substantia nigra is depressed by apomorphine. *Neurosci Lett*. 1984;50(1–3):25–9.
35. Dai M, Tepper JM. Do silent dopaminergic neurons exist in rat substantia nigra in vivo? *Neuroscience*. 1998;85(4):1089–99.
36. Grace AA, Bunney BS. Opposing effects of striatonigral feedback pathways on midbrain dopamine cell activity. *Brain Res*. 1985;333(2):271–84.
37. Björklund A. Dopaminergic transplants in experimental parkinsonism: cellular mechanisms of graft-induced functional recovery. *Curr Opin Neurobiol*. 1992;2(5):683–9.



38. Winkler C, Kirik D, Björklund A, Dunnett SB. Chapter 11 Transplantation in the rat model of Parkinson's disease: ectopic versus homotopic graft placement. In: *Progress in Brain Research* [Internet]. Elsevier; 2000 [cited 2021 Dec 16]. pp. 233–65. Available from: <https://linkinghub.elsevier.com/retrieve/pii/S007961230027012X>
39. Lindvall O, Widner H, Rehnström S, Brundin P, Odin P, Gustavii B, et al. Transplantation of fetal dopamine neurons in Parkinson's disease: One-year clinical and neurophysiological observations in two patients with putaminal implants. *Ann Neurol*. 1992;31(2):155–65.
40. Kordower JH, Freeman TB, Snow BJ, Vingerhoets FJG, Mufson EJ, Sanberg PR, et al. Neuropathological evidence of graft survival and striatal reinnervation after the transplantation of fetal mesencephalic tissue in a patient with Parkinson's disease. *N Engl J Med*. 1995;332(17):1118–24.
41. Piccini P, Brooks DJ, Björklund A, Gunn RN, Grasby PM, Rimoldi O, et al. Dopamine release from nigral transplants visualized in vivo in a Parkinson's patient. *Nat Neurosci*. 1999;2(12):1137–40.
42. Mendez I, Hong M, Smith S, Dagher A, Desrosiers J. Neural transplantation cannula and microinjector system: experimental and clinical experience: technical note. *J Neurosurg*. 2000;92(3):493–9.
43. Björklund A, Parmar M. Dopamine Cell Therapy: From Cell Replacement to Circuitry Repair. Björklund A, Bloem BR, Brundin P, Federoff H, editors. *J Park Dis*. 2021;11(5):S159–65.
44. Thompson LH, Grealish S, Kirik D, Björklund A. Reconstruction of the nigrostriatal dopamine pathway in the adult mouse brain. *Eur J Neurosci*. 2009;30(4):625–38.
45. Droguerre M, Brot S, Vitrac C, Benoit-Marand M, Belnoue L, Patriceon M, et al. Better outcomes with intranigral versus intrastriatal cell transplantation: relevance for Parkinson's disease. *Cells*. 2022;11(7):1191.
46. Brot S, Thamrin NP, Bonnet ML, Francheteau M, Patriceon M, Belnoue L, et al. Long-Term evaluation of intranigral transplantation of human iPSC-Derived dopamine neurons in a Parkinson's disease mouse model. *Cells*. 2022;11(10):1596.
47. Hiller BM, Marmion DJ, Thompson CA, Elliott NA, Federoff H, Brundin P, et al. Optimizing maturity and dose of iPSC-derived dopamine progenitor cell therapy for Parkinson's disease. *Npj Regen Med*. 2022;7(1):24.
48. Adler AF, Cardoso T, Nolbrant S, Mattsson B, Hoban DB, Jarl U, et al. hESC-Derived dopaminergic transplants integrate into basal ganglia circuitry in a preclinical model of Parkinson's disease. *Cell Rep*. 2019;28(13):3462–e34735.
49. Xiong M, Tao Y, Gao Q, Feng B, Yan W, Zhou Y, et al. Human stem Cell-Derived neurons repair circuits and restore neural function. *Cell Stem Cell*. 2021;28(1):112–e1266.
50. Hallett PJ, Deleidi M, Astradsson A, Smith GA, Cooper O, Osborn TM, et al. Successful function of autologous iPSC-Derived dopamine neurons following transplantation in a Non-Human primate model of Parkinson's disease. *Cell Stem Cell*. 2015;16(3):269–74.
51. Kriks S, Shim JW, Piao J, Ganat YM, Wakeman DR, Xie Z, et al. Dopamine neurons derived from human ES cells efficiently engraft in animal models of Parkinson's disease. *Nature*. 2011;480(7378):547–51.
52. Rhee YH, Ko JY, Chang MY, Yi SH, Kim D, Kim CH, et al. Protein-based human iPSC cells efficiently generate functional dopamine neurons and can treat a rat model of Parkinson disease. *J Clin Invest*. 2011;121(6):2326–35.
53. de Luzy IR, Niclis JC, Gantner CW, Kauhausen JA, Hunt CPJ, Ermine C, et al. Isolation of LMX1a ventral midbrain progenitors improves the safety and predictability of human pluripotent stem Cell-Derived neural transplants in parkinsonian disease. *J Neurosci*. 2019;39(48):9521–31.
54. Hao Z, Rajewsky K. Homeostasis of peripheral B cells in the absence of B cell influx from the bone marrow. *J Exp Med*. 2001;194(8):1151–64.
55. Paxinos G, Franklin KBJ. Paxinos and Franklin's the mouse brain in stereotaxic coordinates. Fifth edition. London San Diego Cambridge; MA Kidlington, Oxford: Elsevier, Academic; 2019. p. 326.
56. Guatteo E, Chung KKH, Bowala TK, Bernardi G, Mercuri NB, Lipski J. Temperature sensitivity of dopaminergic neurons of the substantia nigra pars compacta: involvement of transient receptor potential channels. *J Neurophysiol*. 2005;94(5):3069–80.
57. Grace AA, Bunney BS. I intracellular and extracellular electrophysiology of nigral dopaminergic neurons—I. Identif Charact Neurosci. 1983;10(2):301–15.
58. Hyland BI, Reynolds JNJ, Hay J, Perk CG, Miller R. Firing modes of midbrain dopamine cells in the freely moving rat. *Neuroscience*. 2002;114(2):475–92.
59. Ungless MA, Magill PJ, Bolam JP. Uniform Inhibition of dopamine neurons in the ventral tegmental area by aversive stimuli. *Science*. 2004;303(5666):2040–2.
60. Brichoux F, Chakraborty S, Brierley DI, Ungless MA. Phasic excitation of dopamine neurons in ventral VTA by noxious stimuli. *Proc Natl Acad Sci*. 2009;106(12):4894–9.
61. Takahashi YK, Roesch MR, Wilson RC, Toreson K, O'Donnell P, Niv Y, et al. Expectancy-related changes in firing of dopamine neurons depend on orbitofrontal cortex. *Nat Neurosci*. 2011;14(12):1590–7.
62. Pinault D. A novel single-cell staining procedure performed in vivo under electrophysiological control: morpho-functional features of juxtacellularly labeled thalamic cells and other central neurons with Biocytin or neurobiotin. *J Neurosci Methods*. 1996;65(2):113–36.
63. Magill PJ, Bolam JP, Bevan MD. Dopamine regulates the impact of the cerebral cortex on the subthalamic nucleus–globus pallidus network. *Neuroscience*. 2001;106(2):313–30.
64. Bevan MD, Booth PAC, Eaton SA, Bolam JP. Selective innervation of neostriatal interneurons by a subclass of neuron in the globus pallidus of the rat. *J Neurosci*. 1998;18(22):9438–52.
65. Ramayya AG, Zaghoul KA, Weidemann CT, Baltuch GH, Kahana MJ. Electrophysiological evidence for functionally distinct neuronal populations in the human substantia nigra. *Front Hum Neurosci* [Internet]. 2014 Sep 9 [cited 2024 Apr 30];8. Available from: <http://journal.frontiersin.org/article/;https://doi.org/10.3389/fnhum.2014.00655/abstract>
66. Zaghoul KA, Blanco JA, Weidemann CT, McGill K, Jaggi JL, Baltuch GH, et al. Hum Substantia Nigra Neurons Encode Unexpected Financial Rewards Sci. 2009;323(5920):1496–9.
67. de Vrind V, Scuvée-Moreau J, Drion G, Hmaied C, Philippart F, Engel D, et al. Interactions between calcium channels and SK channels in midbrain dopamine neurons and their impact on pacemaker regularity: contrasting roles of N- and L-type channels. *Eur J Pharmacol*. 2016;788:274–9.
68. Grace AA, Bunney BS. The control of firing pattern in nigral dopamine neurons: burst firing. *J Neurosci Off J Soc Neurosci*. 1984;4(11):2877–90.
69. Shepard PD, German DC. Electrophysiological and Pharmacological evidence for the existence of distinct subpopulations of nigrostriatal dopaminergic neuron in the rat. *Neuroscience*. 1988;27(2):537–46.
70. Grenhoff J, Svensson TH. Clonidine regularizes substantia nigra dopamine cell firing. *Life Sci*. 1988;42(20):2003–9.
71. Miller JD, Sanghera MK, German DC. Mesencephalic dopaminergic unit activity in the behaviorally conditioned rat. *Life Sci*. 1981;29(12):1255–63.
72. Schultz W. Predictive reward signal of dopamine neurons. *J Neurophysiol*. 1998;80(1):1–27.
73. Seutin V, Massotte L, Renette MF, Dresse A. Evidence for a modulatory role of ih on the firing of a subgroup of midbrain dopamine neurons. *NeuroReport*. 2001;12(2):255–8.
74. Kitai ST, Shepard PD, Callaway JC, Scroggs R. Afferent modulation of dopamine neuron firing patterns. *Curr Opin Neurobiol*. 1999;9(6):690–7.
75. Grace A, Onn S. Morphology and electrophysiological properties of immunocytochemically identified rat dopamine neurons recorded in vitro. *J Neurosci*. 1989;9(10):3463–81.
76. Kang Y, Kitai ST. A whole cell patch-clamp study on the pacemaker potential in dopaminergic neurons of rat substantia nigra compacta. *Neurosci Res*. 1993;18(3):209–21.
77. Llinás R, Yarom Y. Oscillatory properties of guinea-pig inferior olivary neurones and their Pharmacological modulation: an in vitro study. *J Physiol*. 1986;376(1):163–82.
78. Grillner S. Locomotion in vertebrates: central mechanisms and reflex interaction. *Physiol Rev*. 1975;55(2):247–304.
79. Ishiwa D, Kamiya Y, Itoh H, Saito Y, Ohtsuka T, Yamada Y, et al. Effects of isoflurane and ketamine on ATP-sensitive K channels in rat substantia nigra. *Neuropharmacology*. 2004;46(8):1201–12.
80. Liss B. Tuning pacemaker frequency of individual dopaminergic neurons by Kv4.3L and KChip3.1 transcription. *EMBO J*. 2001;20(20):5715–24.
81. Ishiwa D, Nagata I, Ohtsuka T, Itoh H, Kamiya Y, Ogawa K, et al. Differential effects of isoflurane on A-type and delayed rectifier K channels in rat substantia nigra. *Eur J Pharmacol*. 2008;580(1–2):122–9.
82. Grace A, Bunney B. The control of firing pattern in nigral dopamine neurons: single Spike firing. *J Neurosci*. 1984;4(11):2866–76.
83. Paladini CA, Tepper JM. GABAA and GABAB antagonists differentially affect the firing pattern of substantia nigra dopaminergic neurons in vivo. *Synapse*. 1999;32(3):165–76.
84. Grace AA, Floresco SB, Goto Y, Lodge DJ. Regulation of firing of dopaminergic neurons and control of goal-directed behaviors. *Trends Neurosci*. 2007;30(5):220–7.

85. Seutin V, Johnson SW, North RA. Apamin increases NMDA-induced burst-firing of rat mesencephalic dopamine neurons. *Brain Res.* 1993;630(1–2):341–4.
86. Gu X, Blatz AL, German DC. Subtypes of substantia nigra dopaminergic neurons revealed by Apamin: autoradiographic and electrophysiological studies. *Brain Res Bull.* 1992;28(3):435–40.
87. Gantz SC, Ford CP, Morikawa H, Williams JT. The evolving Understanding of dopamine neurons in the substantia nigra and ventral tegmental area. *Annu Rev Physiol.* 2018;80(1):219–41.
88. Chergui K, Charléty PJ, Akaoka H, Saunier CF, Brunet JL, Buda M, et al. Tonic activation of NMDA receptors causes spontaneous burst discharge of rat midbrain dopamine neurons *In vivo*. *Eur J Neurosci.* 1993;5(2):137–44.
89. Watabe-Uchida M, Zhu L, Ogawa SK, Vamanrao A, Uchida N. Whole-Brain mapping of direct inputs to midbrain dopamine neurons. *Neuron.* 2012;74(5):858–73.
90. Kita H, Kitai ST. Efferent projections of the subthalamic nucleus in the rat: light and electron microscopic analysis with the PHA-L method. *J Comp Neurol.* 1987;260(3):435–52.
91. Floresco SB, West AR, Ash B, Moore H, Grace AA. Afferent modulation of dopamine neuron firing differentially regulates tonic and phasic dopamine transmission. *Nat Neurosci.* 2003;6(9):968–73.
92. Cardoso T, Adler AF, Mattsson B, Hoban DB, Nolbrant S, Wahlestedt JN, et al. Target-specific forebrain projections and appropriate synaptic inputs of hESC-derived dopamine neurons grafted to the midbrain of parkinsonian rats. *J Comp Neurol.* 2018;526(13):2133–46.
93. Balcita-Pedicino JJ, Omelchenko N, Bell R, Sesack SR. The inhibitory influence of the lateral Habenula on midbrain dopamine cells: ultrastructural evidence for indirect mediation via the Rostromedial mesopontine tegmental nucleus. *J Comp Neurol.* 2011;519(6):1143–64.
94. Matsumoto M, Hikosaka O. Two types of dopamine neuron distinctly convey positive and negative motivational signals. *Nature.* 2009;459(7248):837–41.
95. Lobb CJ, Troyer TW, Wilson CJ, Paladini CA. Disinhibition Bursting of Dopaminergic Neurons. *Front Syst Neurosci* [Internet]. 2011 [cited 2021 Dec 17];5. Available from: <http://journal.frontiersin.org/article/https://doi.org/10.3389/fnys.2011.00025/abstract>
96. Beaulieu-Laroche L, Toloza EHS, Van Der Goes MS, Lafourcade M, Barnagian D, Williams ZM, et al. Enhanced dendritic compartmentalization in human cortical neurons. *Cell.* 2018;175(3):643–e65114.
97. Libé-Philippot B, Lejeune A, Wierda K, Louros N, Erkol E, Vlaeminck I, et al. LRRRC37B is a human modifier of voltage-gated sodium channels and axon excitability in cortical neurons. *Cell.* 2023;186(26):5766–e578325.
98. Ferguson KA, Cardin JA. Mechanisms underlying gain modulation in the cortex. *Nat Rev Neurosci.* 2020;21(2):80–92.
99. Beck H, Yaari Y. Plasticity of intrinsic neuronal properties in CNS disorders. *Nat Rev Neurosci.* 2008;9(5):357–69.
100. Krashia P, Martini A, Nobili A, Aversa D, D'Amelio M, Berretta N, et al. On the properties of identified dopaminergic neurons in the mouse substantia nigra and ventral tegmental area. *Eur J Neurosci.* 2017;45(1):92–105.
101. Burkert N, Roy S, Häusler M, Wuttke D, Müller S, Wiemer J, et al. Deep learning-based image analysis identifies a DAT-negative subpopulation of dopaminergic neurons in the lateral substantia nigra. *Commun Biol.* 2023;6(1):1146.
102. Farassat N, Costa KM, Stojanovic S, Albert S, Kovacheva L, Shin J, et al. In vivo functional diversity of midbrain dopamine neurons within identified axonal projections. *eLife.* 2019;8:e48408.
103. Grealish S, Diguett E, Kirkeby A, Mattsson B, Heuer A, Bramouille Y, et al. Human ESC-Derived dopamine neurons show similar preclinical efficacy and potency to fetal neurons when grafted in a rat model of Parkinson's disease. *Cell Stem Cell.* 2014;15(5):653–65.
104. Sierra A, Encinas JM, Maletic-Savatic M. Adult Human Neurogenesis: From Microscopy to Magnetic Resonance Imaging. *Front Neurosci* [Internet]. 2011 [cited 2024 Jul 15];5. Available from: <http://journal.frontiersin.org/article/https://doi.org/10.3389/fnins.2011.00047/abstract>
105. Stiles J, Jernigan TL. The basics of brain development. *Neuropsychol Rev.* 2010;20(4):327–48.
106. Silbereis JC, Pochareddy S, Zhu Y, Li M, Sestan N. The cellular and molecular landscapes of the developing human central nervous system. *Neuron.* 2016;89(2):248–68.
107. Zhao C, Deng W, Gage FH. Mechanisms and functional implications of adult neurogenesis. *Cell.* 2008;132(4):645–60.

## Publisher's note

Springer Nature remains neutral with regard to jurisdictional claims in published maps and institutional affiliations.